

UC San Diego

UC San Diego Previously Published Works

Title

A self-consistent phase-field approach to implicit solvation of charged molecules with Poisson–Boltzmann electrostatics

Permalink

<https://escholarship.org/uc/item/1df8x4h9>

Journal

The Journal of Chemical Physics, 143(24)

ISSN

0021-9606

Authors

Sun, Hui

Wen, Jiayi

Zhao, Yanxiang

et al.

Publication Date

2015-12-28

DOI

10.1063/1.4932336

Peer reviewed

A self-consistent phase-field approach to implicit solvation of charged molecules with Poisson–Boltzmann electrostatics

Hui Sun,^{1,a),b)} Jiayi Wen,^{1,a),c)} Yanxiang Zhao,^{2,a),d)} Bo Li,^{3,e)} and J. Andrew McCammon^{4,f)}

¹*Department of Mathematics, University of California, San Diego, 9500 Gilman Drive, Mail Code 0112, La Jolla, California 92093-0112, USA*

²*Department of Mathematics, the George Washington University, Monroe Hall, 2115 G St. NW, Washington, DC 20052, USA*

³*Department of Mathematics and Quantitative Biology Graduate Program, University of California, San Diego, 9500 Gilman Drive, Mail Code 0112, La Jolla, California 92093-0112, USA*

⁴*Department of Chemistry and Biochemistry, Department of Pharmacology, and Howard Hughes Medical Institute, University of California, San Diego, La Jolla, California 92093-0365, USA*

(Received 6 August 2015; accepted 22 September 2015; published online 8 October 2015)

Dielectric boundary based implicit-solvent models provide efficient descriptions of coarse-grained effects, particularly the electrostatic effect, of aqueous solvent. Recent years have seen the initial success of a new such model, variational implicit-solvent model (VISM) [Dzubiella, Swanson, and McCammon *Phys. Rev. Lett.* **96**, 087802 (2006) and *J. Chem. Phys.* **124**, 084905 (2006)], in capturing multiple dry and wet hydration states, describing the subtle electrostatic effect in hydrophobic interactions, and providing qualitatively good estimates of solvation free energies. Here, we develop a phase-field VISM to the solvation of charged molecules in aqueous solvent to include more flexibility. In this approach, a stable equilibrium molecular system is described by a phase field that takes one constant value in the solute region and a different constant value in the solvent region, and smoothly changes its value on a thin transition layer representing a smeared solute-solvent interface or dielectric boundary. Such a phase field minimizes an effective solvation free-energy functional that consists of the solute-solvent interfacial energy, solute-solvent van der Waals interaction energy, and electrostatic free energy described by the Poisson–Boltzmann theory. We apply our model and methods to the solvation of single ions, two parallel plates, and protein complexes BphC and p53/MDM2 to demonstrate the capability and efficiency of our approach at different levels. With a diffuse dielectric boundary, our new approach can describe the dielectric asymmetry in the solute-solvent interfacial region. Our theory is developed based on rigorous mathematical studies and is also connected to the Lum–Chandler–Weeks theory (1999). We discuss these connections and possible extensions of our theory and methods. © 2015 AIP Publishing LLC. [<http://dx.doi.org/10.1063/1.4932336>]

I. INTRODUCTION

Aqueous solvent plays a central role in biological molecular processes such as conformational change, molecular recognition, and molecular assembly.^{1–6} Detailed descriptions of individual solvent molecules, however, can be very costly due to the large number of such molecules necessary to be included in an underlying system. Dielectric boundary based implicit-solvent models^{7–12} provide efficient descriptions of coarse-grained effects, particularly the electrostatic effect, of aqueous solvent through a few macroscopic parameters such as the surface tension, dielectric coefficients, bulk solvent density, and bulk ionic concentrations. In such a model, one first determines a dielectric boundary that separates a charged molecular region from the solvent region, with the dielectric coefficients of these regions close to 1 and 80, respectively, and then applies the

Poisson–Boltzmann (PB) theory^{13–24} or the generalized Born (GB) model^{25,26} to calculate the electrostatic free energy.

The question here is how to define and computationally determine a dielectric boundary as it is critical to the free-energy estimation. For instance, the classical Born model²⁷ predicts the free energy of hydration of a single ion in water to be inversely proportional to an effective radius of the ion; any relative error in such a radius will therefore lead to a relative error of same order in the free-energy estimation. For a biological molecule such as a protein, one can efficiently generate a dielectric boundary as a van der Waals surface (vdWS), solvent-excluded surface (SES), or solvent-accessible surface (SAS),^{28–32} leaving though many parameters to adjust. Moreover, in calculating the surface energy that is an important component of the total free energy with such a fixed surface, a curvature correction³³ to surface tension can hardly be made systematically. Such correction is known to be crucial, as cavitation free energies do not scale with surface area for high curvatures.^{34–38} A more subtle and important situation occurs around a hydrophobic pocket, a region inside or on the surface of a protein where a few water molecules fluctuate, making dry-wet transitions. Experiment and molecular

^{a)}H. Sun, J. Wen, and Y. Zhao contributed equally to this work.

^{b)}Electronic mail: hus003@ucsd.edu

^{c)}Electronic mail: wen.jiayi.thomas@gmail.com

^{d)}Electronic mail: yxzhao@email.gwu.edu

^{e)}Electronic mail: bli@math.ucsd.edu

^{f)}Electronic mail: jmccammon@ucsd.edu

dynamics (MD) simulations have suggested that such pockets and the associated dry-wet transitions are crucial in protein-ligand binding, and molecular recognition in general.^{39–58} As the size of such a pocket is large enough to contain a few water molecules, it is evident that the fluctuating pocket surface can be hardly described by any kinds of fixed surfaces.

In general, determining a dielectric boundary requires taking into account multi-body effects, including solute-solvent interactions, solute charge and solvent polarization effects, and many others. This is exactly one of the principles behind a recently developed, dielectric boundary based, implicit-solvent model: variational implicit-solvent model (VISM).^{59,60} In VISM, one minimizes a macroscopic, mean-field free-energy functional of all possible solute-solvent interfaces or dielectric boundaries. The free-energy functional consists of surface energy, solute excluded volume and solute-solvent vdW interaction energy, and continuum electrostatic free energy, all coupled together through a given solute-solvent interface, i.e., dielectric boundary. Moreover, the curvature correction to surface tension can be systematically incorporated in the VISM free-energy functional. Minimization of the functional determines the solvation free energy and stable equilibrium solute-solvent interfaces. Computationally, such minimization can be realized by a robust level-set numerical method.^{61–65} Extensive level-set computational results with comparison to experiment and MD simulations have demonstrated the success of this new approach to the solvation of charged molecular systems in capturing efficiently different hydration states, providing qualitatively good estimates of solvation free energies, and describing subtle electrostatic effects; cf. Refs. 61–72. In general, stable equilibrium solute-solvent interfaces determined by the level-set VISM can be quite different from vdWS, SES, or SAS, particularly when it comes to the description of hydrophobic interactions.^{1,2,39,73–77} Perhaps, the most significant feature of VISM is that its free-energy functional exhibits a complex energy landscape with multiple local minima corresponding to different equilibrium hydration states.

We notice that several related issues, such as coupling the solvent boundary to optimization of overall energy, the curvature effect to surface energy, and dewetting transition, have been discussed in the literature; and the related models and methods have also been proposed.^{10,12,36,45,78–80}

In this work, we develop a phase-field variational implicit-solvent model (PF-VISM) with the PB electrostatics. It is an alternative to the original VISM that uses a sharp-interface formulation, and it extends our previous work^{81,82} that only used the Coulomb-field approximation (CFA) of electrostatic free energy. We aim at making these approaches more flexible in describing possibly detailed solute-solvent interfacial structures, and introducing fluctuations in the future.

The phase-field theory and methods have been widely used to study many interfacial problems in materials physics, complex fluids, biomembranes, and other scientific areas; cf., e.g., Refs. 83–94 and the references therein. The key idea here is to describe a diffuse interface that separates two regions by a smooth function ϕ , called a phase field, that takes its value close to one constant in one of the regions and another constant in the other region, but smoothly changes its value from one of the constants to another in a thin transition layer, forming the

diffuse interface. The area of such an interface is approximated by the phase-field area $S_\xi[\phi]$, defined by

$$S_\xi[\phi] = \int \left[\frac{\xi}{2} |\nabla\phi|^2 + \frac{1}{\xi} W(\phi) \right] d\mathbf{x},$$

where $\xi > 0$ is a small parameter characterizing the width of transition layer and W is a properly chosen double-well potential, e.g., $W(\phi) = 18\phi^2(1 - \phi)^2$. If the surface area $S_\xi[\phi]$ is small, then the W -term forces the phase field ϕ to be close to the two wells of W , partitioning the entire system into two regions with a thin transition layer, and the gradient term penalizes such partition. In our case, these two regions are the solvent region $\{\phi \approx 0\}$ and solute region $\{\phi \approx 1\}$, respectively, and the thin transition layer is the diffuse solute-solvent interface. As the parameter ξ becomes smaller and smaller, the transition layer converges to a sharp interface and the corresponding integral value converges to the interfacial area.^{81,95,96} This well established mathematical theory is the foundation of the phase-field approach. Note that, in terms of the mathematical form, the integral $S_\xi[\phi]$ is exactly the first term of the Hamiltonian of large-scale solvent density in the Lum–Chandler–Weeks theory⁹⁷ for hydrophobic interactions.

We minimize our PF-VISM free-energy functional to determine a stable equilibrium molecular conformation and its corresponding solvation free energy. As in the sharp-interface VISM, our total solvation free-energy functional consists of three parts: (1) The surface energy $\gamma_0 S_\xi[\phi]$ with γ_0 an effective surface tension; (2) The solute-solvent interaction energy determined by the bulk water density ρ_w and the Lennard-Jones (LJ) parameters for the individual solute-solvent pairwise interactions; and (3) The electrostatic free energy determined by the PB theory in which the dielectric coefficient $\varepsilon = \varepsilon(\phi)$ depends smoothly on the phase field ϕ and takes the solvent and solute dielectric coefficients for $\phi \approx 0$ and $\phi \approx 1$, respectively. Note that we have not directly included the curvature correction to the surface tension, for otherwise, such inclusion can be computationally costly. Rather, we tune the effective parameters γ_0 ad ξ to make our free-energy calculations more accurate. Note also that we shall use the linearized PB equation as we consider charged molecules in a dilute aqueous solution.

One of the new features of our PF-VISM with the PB electrostatics is its flexibility in the detailed description of the dielectric environment in the thin solute-solvent interfacial layer.⁹⁸ This is related to the basic issue of defining a dielectric boundary. There are different kinds of solute-solvent interfaces; and most of them are defined using the fluctuating solvent density.^{99,100} Such an interface can be conceptually different from a dielectric boundary defined as a sharp surface that separates the solute region with one dielectric constant from the solvent region with another dielectric constant. In our previous VISM calculations, after we minimized the free-energy functional, we shifted the free-energy minimizing dielectric boundary inward to the solute to finally calculate the electrostatic free energy. We found that such a boundary shift provided better results on electrostatics in comparison with experiment and MD simulations.^{65,67,69,70} Similarly, calculations reported in Ref. 101 show that a tight vdWS is a better dielectric boundary than a molecular surface (i.e., SES). In our PF-VISM, we construct analytic forms of the dielectric

coefficient $\varepsilon = \varepsilon(\phi)$ to mimic experimental data, allowing the asymmetry with respect to $\phi \approx 0$ for the solvent region and $\phi \approx 1$ for the solute region.⁹⁸ We shall demonstrate that this may be a first step toward a detailed description of solute-solvent interfacial structures using an implicit-solvent approach.

To minimize our PF-VISM free-energy functional $F_\xi[\phi]$, where the PB equation for the electrostatic potential $\psi = \psi_\phi$ is a constraint, we solve numerically the gradient-flow (i.e., relaxation dynamics) partial differential equations $\partial_t \phi = -\delta_\phi F_\xi[\phi]$ together with the PB equation for ψ_ϕ that depends now on the phase field ϕ through mainly the dielectric coefficient $\varepsilon = \varepsilon(\phi)$. In our recent mathematical work,¹⁰² we derived rigorously the first variation $\delta_\phi F_\xi[\phi]$ and also proved that in the sharp-interface limit as $\xi \rightarrow 0$, our phase-field relaxation dynamics converges to the sharp-interface VISM relaxation dynamics. Here, we first present the main steps in the calculation of first variation for the electrostatic part of the free energy. We then use an implicit scheme for the Laplacian of ϕ and other linear terms and an explicit scheme for nonlinear terms in the time discretization of the gradient-flow partial differential equations. In each time step, we solve several systems of linear equations with the preconditioning conjugate gradient method. These schemes and methods are shown to be convergent in the expected order. In coding our algorithms, we used the computational software PETSc.¹⁰³

We apply our theory and method to several charged molecular systems of different complexities. First, we consider the hydration of some single ions and compare our phase-field calculations with experimental results. Notice that it is in general difficult to experimentally measure the ionic hydration free energy and effective radius for a single ion. The experimental data (a lot, if not all), reported in the past century and collected in Ref. 104, seem so dispersive. We shall demonstrate that, with reasonable adjustment of certain parameters, our approach can provide good estimates of hydration free energies for single ions. Second, we consider two parallel, initially hydrophobic plates, where the plate charge is a free parameter and gradually increased. We study the influence of charging on the hydrophobic interactions, the system balance between dry and wet equilibrium states, and the resulting hysteresis in the potential of mean force. Third, we consider two real protein systems. One is the two domain protein BphC and the other is the protein complex p53/MDM2. For each of these systems, we show the charge effect captured by our approach and also the difference between our PF-VISM dielectric boundary and a vdWS. In all of our computations, we do not shift our phase-field dielectric boundary.

We organize the rest of our paper as follows: In Section II, we present our phase-field solvation free-energy functional and derive its first variations. In Section III, we describe our numerical methods for solving the gradient-flow partial differential equations for minimizing the free-energy functional. In Section IV, we present our computational results for single ions, two charged plates, the two-domain protein BphC, and the protein complex p53/MDM2. Finally, in Section V, we draw conclusions of our studies, discuss several issues of our approach, and point out some possible extensions.

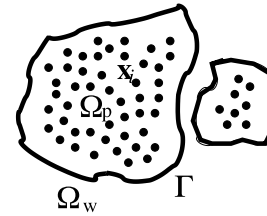


FIG. 1. A schematic description of a solvation system. A solute-solvent interface Γ divides the entire solvation region Ω into the solute region Ω_p and solvent region Ω_w . Solid dots represent solute atoms, located at \mathbf{x}_i and carrying partial charges Q_i ($1 \leq i \leq N$), respectively.

II. THEORY

We consider the solvation of a charged molecule (or a group of charged molecules) in aqueous solvent and assume that the solvation system occupies a bounded region $\Omega \subset \mathbb{R}^3$. This region is divided into the solute region Ω_p (p stands for protein) that contains all the solute atoms, the solvent region Ω_w (w stands for water), and a thin transition layer that is a smeared solute-solvent interface Γ , cf. Fig. 1. We assume that there are N solute atoms, located at $\mathbf{x}_i \in \Omega$ and carrying partial charges Q_i ($1 \leq i \leq N$), respectively. These atoms are assumed to be fixed as we only consider here the equilibrium properties of the solvation system.

A. Free-energy functional

Let $\xi > 0$ be a small, numerical parameter with the unit of length that characterizes the size of solute-solvent transition layer. We minimize the following effective, solvation free-energy functional of phase field $\phi = \phi(\mathbf{x})$:

$$F_\xi[\phi] = F_{\text{geom},\xi}[\phi] + F_{\text{vdw}}[\phi] + F_{\text{ele}}[\phi], \quad (2.1)$$

where

$$\begin{aligned} F_{\text{geom},\xi}[\phi] &= P \int_{\Omega} \phi^2 d\mathbf{x} + \gamma_0 \int_{\Omega} \left[\frac{\xi}{2} |\nabla \phi|^2 + \frac{1}{\xi} W(\phi) \right] d\mathbf{x}, \\ F_{\text{vdw}}[\phi] &= \rho_w \int_{\Omega} (\phi - 1)^2 U_{\text{vdw}} d\mathbf{x}, \\ F_{\text{ele}}[\phi] &= F_{\text{ele}}^{\text{PB}}[\phi] = \frac{1}{2} \sum_{i=1}^N Q_i \psi_{\text{reac},\phi}(\mathbf{x}_i) \\ &\quad + \int_{\Omega} (\phi - 1)^2 \left[\frac{1}{2} \psi_\phi V'(\psi_\phi) - V(\psi_\phi) \right] d\mathbf{x}. \end{aligned}$$

The geometrical part $F_{\text{geom},\xi}[\phi]$ consists of two terms. In the first term, P is the difference between the solvent liquid pressure and solute vapor pressure. The integral term approximates the volume of solute region described by $\phi \approx 1$ for a phase field ϕ with a low free energy. Note that this term is usually very small compared with the others and is therefore often neglected. (We shall set $P = 0$ in this work.) The second term in $F_{\text{geom},\xi}[\phi]$ describes the solute-solvent interfacial energy, where γ_0 is an effective surface tension and $W(\phi) = 18\phi^2(1 - \phi)^2$. If the free energy $F_\xi[\phi]$ is small, then the W -term forces the phase field ϕ to be close to 0 or 1 in the entire solvation region Ω , with $\{\phi \approx 1\}$ and $\{\phi \approx 0\}$ the solute and solvent regions, respectively, except a thin transition layer. The van der Waals (vdW) part $F_{\text{vdw}}[\phi]$, in which ρ_w is the bulk

solvent density, describes the solute-solvent interaction that includes both the solute excluded volume and solute-solvent vdW attraction. We take the potential $U_{\text{vdW}} = U_{\text{vdW}}(\mathbf{x})$ to be the sum of pairwise interactions $U_{\text{vdW}}(\mathbf{x}) = \sum_{i=1}^N U_{\text{LJ}}^{(i)}(|\mathbf{x} - \mathbf{x}_i|)$, where $U_{\text{LJ}}^{(i)}(r) = 4\epsilon_i [(\sigma_i/r)^{12} - (\sigma_i/r)^6]$ is the LJ potential for the interaction of the i th solute particle and a solvent molecule or ion. The term $(\phi - 1)^2$ in the integrand indicates that the integral is over the solvent region $\{\phi \approx 0\}$.

Finally, the electrostatic free energy $F_{\text{ele}}[\phi]$ or $F_{\text{ele}}^{\text{PB}}[\phi]$ is defined by the PB theory. In $F_{\text{ele}}^{\text{PB}}[\phi]$, ψ_ϕ is the electrostatic potential. It is the unique solution to the boundary-value problem of PB equation in the phase-field formulation

$$-\nabla \cdot \epsilon(\phi) \nabla \psi_\phi + (\phi - 1)^2 V'(\psi_\phi) = \rho_f \quad \text{in } \Omega, \quad (2.2)$$

$$\psi_\phi = \psi_\infty \quad \text{on } \partial\Omega, \quad (2.3)$$

where $\rho_f(\mathbf{x}) = \sum_{i=1}^N Q_i \delta(\mathbf{x} - \mathbf{x}_i)$ is the solute point charge density and ψ_∞ is a given function. In $F_{\text{ele}}^{\text{PB}}[\phi]$, $\psi_{\text{reac},\phi} = \psi_\phi - \psi_{\text{vac}}$ is the reaction field, and $\psi_{\text{vac}}(\mathbf{x}) = \sum_{i=1}^N Q_i / (4\pi\epsilon_p\epsilon_0|\mathbf{x} - \mathbf{x}_i|)$ is the electrostatic potential in the reference state with ϵ_p the solute dielectric coefficient and ϵ_0 the vacuum permittivity. Since $-\epsilon_p\epsilon_0\Delta\psi_{\text{vac}} = \rho_f$ and $\psi_{\text{vac}}(\infty) = 0$, we can reformulate the boundary-value problem of PB equation into

$$-\nabla \cdot \epsilon(\phi) \nabla \psi_{\text{reac},\phi} + (\phi - 1)^2 V'(\psi_{\text{reac},\phi} + \psi_{\text{vac}}) = \nabla \cdot [\epsilon(\phi) - \epsilon_p\epsilon_0] \nabla \psi_{\text{vac}} \quad \text{in } \Omega, \quad (2.4)$$

$$\psi_{\text{reac},\phi} = \psi_\infty - \psi_{\text{vac}} \quad \text{on } \partial\Omega. \quad (2.5)$$

The function $V = V(\psi_\phi)$ in $F_{\text{ele}}[\phi]$, Eq. (2.2), and Eq. (2.4) is given by

$$V(\psi_\phi) = \begin{cases} \beta^{-1} \sum_{j=1}^M c_j^\infty (e^{-\beta q_j \psi_\phi} - 1) & \text{for nonlinear PB,} \\ \frac{1}{2} \epsilon_w \epsilon_0 \kappa^2 \psi_\phi^2 & \text{for linearized PB,} \end{cases}$$

where $\beta = 1/(k_B T)$ with k_B the Boltzmann constant and T the temperature, $q_j = Z_j e$ with e the elementary charge, and Z_j and c_j^∞ are the valence and bulk concentrations of the j th ionic species, respectively, and κ is the inverse Debye length, $\kappa^2 = (\beta/\epsilon_w\epsilon_0) \sum_{j=1}^M c_j^\infty q_j^2$. Here, we assume there are M ionic species. Note for the linearized PB that the integral term in the free energy $F_{\text{ele}}^{\text{PB}}[\phi]$ vanishes.

The phase-field dielectric coefficient $\epsilon(\phi)$ is a smooth and monotonic function of ϕ such that $\epsilon(\phi) = \epsilon_p\epsilon_0$ if $\phi \geq 1$ and $\epsilon(\phi) = \epsilon_w\epsilon_0$ if $\phi \leq 0$, where ϵ_w is the solvent dielectric coefficient. An example of such a function is¹⁰²

$$\epsilon(\phi) = \begin{cases} \epsilon_w\epsilon_0 & \text{if } \phi \leq 0, \\ \frac{\epsilon_p\epsilon_0 e^{\tan(\pi(\phi-1/2))} + \epsilon_w\epsilon_0 e^{-\tan(\pi(\phi-1/2))}}{e^{\tan(\pi(\phi-1/2))} + e^{-\tan(\pi(\phi-1/2))}} & \text{if } 0 < \phi < 1, \\ \epsilon_p\epsilon_0 & \text{if } \phi \geq 1. \end{cases} \quad (2.6)$$

Note that the profile of $\epsilon = \epsilon(\phi)$ is rather symmetric, cf. Fig. 2 (left). However, it is known experimentally⁹⁸ that the profile of dielectric coefficient in the region of transition from charges to aqueous ionic solution is not symmetric, cf. Fig. 2 (right). Therefore, we introduce two adjustable parameters ϕ_p and ϕ_w such that $0 \leq \phi_w < \phi_p \leq 1$ and define the corresponding, shifted, phase-field dielectric coefficient by

$$\epsilon_{\text{Shift}}(\phi) = \epsilon \left(\frac{\phi - \phi_w}{\phi_p - \phi_w} \right). \quad (2.7)$$

Based on experiment,⁹⁸ we often choose $\phi_w > 0$ (e.g., $\phi_w = 0.25$ or 0.33) and $\phi_p = 1$. Fig. 2 shows the profile of the original $\epsilon = \epsilon(\phi)$ defined in (2.6) and that of a shifted one with $\phi_w = 1/3$ and $\phi_p = 1$, respectively.

We recall the CFA of electrostatic free energy,^{67,81,82,105}

$$F_{\text{ele}}^{\text{CFA}}[\phi] = \int_{\Omega} (\phi - 1)^2 U_{\text{CFA}} d\mathbf{x}, \quad (2.8)$$

where the term $(\phi - 1)^2$ indicates again that the integral is over the solvent region $\{\phi \approx 0\}$ and

$$U_{\text{CFA}}(\mathbf{x}) = \frac{1}{32\pi^2\epsilon_0} \left(\frac{1}{\epsilon_w} - \frac{1}{\epsilon_p} \right) \left| \sum_{i=1}^N \frac{Q_i(\mathbf{x} - \mathbf{x}_i)}{|\mathbf{x} - \mathbf{x}_i|^3} \right|^2. \quad (2.9)$$

Note that the ionic effect is neglected in the CFA. Here, we shall use the CFA to speed up our computations, as it does not require the solution of any partial differential equations.

B. First variation and relaxation dynamics

We minimize free-energy functional (2.1) by solving the equation of relaxation dynamics $\partial_t \phi = -\delta_\phi F_\xi[\phi]$ for

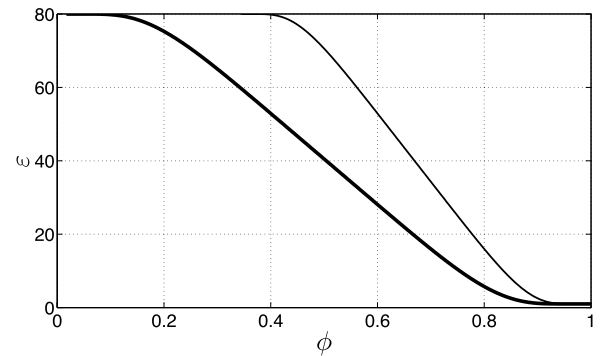


FIG. 2. Thick curve is the profile of the original, symmetric phase-field dielectric coefficient $\epsilon = \epsilon(\phi)$ defined in (2.6). Thin curve is the profile of an asymmetric phase-field dielectric coefficient $\epsilon = \epsilon(\phi)$ defined in (2.7) with $\phi_w = 1/3$ and $\phi_p = 1$.

$\phi = \phi(\mathbf{x}, t)$, together with PB equation (2.4), to obtain an equilibrium solution for which $\phi = 1/2$ determines the solute-solvent interface and $F_\xi[\phi]$ is the solvation free energy for the equilibrium conformation.

To calculate the first variation $\delta_\phi F_\xi[\phi]$, we first approximate the point charges $\rho_f = \sum_{i=1}^N Q_i \delta_{\mathbf{x}_i}$ by the sum of Gaussian type functions centered at solute atoms \mathbf{x}_i ($1 \leq i \leq N$). We denote still by ρ_f this smoothed solute charge density. The potential ψ_ϕ with such a smoothed charge density is no longer singular at \mathbf{x}_i ($1 \leq i \leq N$). In the same way, we smooth out the reference potential ψ_{vac} . We now rewrite the PB electrostatic free energy $F_{\text{ele}}^{\text{PB}}[\phi]$. Multiplying both sides of PBE (2.2) by ψ_ϕ and integrating them over Ω using integration by parts, we obtain with appropriate boundary conditions

that

$$\int_{\Omega} [\varepsilon(\phi) |\nabla \psi_\phi|^2 + (\phi - 1)^2 \psi_\phi V'(\psi_\phi)] d\mathbf{x} = \langle \rho_f, \psi_\phi \rangle, \quad (2.10)$$

where the right-hand side denotes $\sum_{i=1}^N Q_i \psi_\phi(\mathbf{x}_i)$. Applying this to $-\langle \rho_f, \psi_\phi \rangle/2$, we have

$$F_{\text{ele}}^{\text{PB}}[\phi] = -\frac{1}{2} \langle \rho_f, \psi_{\text{vac}} \rangle + \langle \rho_f, \psi_\phi \rangle - \int_{\Omega} \left[\frac{\varepsilon(\phi)}{2} |\nabla \psi_\phi|^2 + (\phi - 1)^2 V(\psi_\phi) \right] d\mathbf{x}.$$

Denoting by $\delta\phi$ and $\delta_\phi \psi_\phi$, respectively, the variations of ϕ and ψ_ϕ with respect to ϕ , we then obtain by (2.1) and the Chain Rule that

$$\begin{aligned} \delta_\phi F_\xi[\phi] \delta\phi &= \int_{\Omega} \left[2P\phi - \gamma_0 \xi \Delta\phi + \frac{\gamma_0}{\xi} W'(\phi) + 2\rho_w(\phi - 1) U_{\text{vdW}} \right] \delta\phi d\mathbf{x} + \int_{\Omega} \left[-\frac{\varepsilon'(\phi)}{2} |\nabla \psi_\phi|^2 - 2(\phi - 1)V(\psi_\phi) \right] \delta\phi d\mathbf{x} \\ &\quad + \langle \rho_f, \delta_\phi \psi_\phi \rangle + \int_{\Omega} [\nabla \cdot \varepsilon(\phi) \nabla \psi_\phi - (\phi - 1)^2 V'(\psi_\phi)] \delta_\phi \psi_\phi d\mathbf{x} \\ &= \int_{\Omega} \left[2P\phi - \gamma_0 \xi \Delta\phi + \frac{\gamma_0}{\xi} W'(\phi) + 2\rho_w(\phi - 1) U_{\text{vdW}} - \frac{\varepsilon'(\phi)}{2} |\nabla \psi_\phi|^2 - 2(\phi - 1)V(\psi_\phi) \right] \delta\phi d\mathbf{x}, \end{aligned} \quad (2.11)$$

where in the last step, we used (2.10). Consequently,

$$\begin{aligned} \delta_\phi F_\xi[\phi] &= 2P\phi - \gamma_0 \xi \Delta\phi + \frac{\gamma_0}{\xi} W'(\phi) \\ &\quad + 2\rho_w(\phi - 1) U_{\text{vdW}} - \frac{\varepsilon'(\phi)}{2} |\nabla \psi_\phi|^2 \\ &\quad - 2(\phi - 1)V(\psi_\phi). \end{aligned}$$

To summarize, we shall solve numerically the following initial-boundary-value problem for $\phi = \phi(\mathbf{x}, t)$ and $\psi = \psi(\mathbf{x}, t)$:

$$\begin{aligned} \partial_t \phi &= -2P\phi + \gamma_0 \left[\xi \Delta\phi - \frac{1}{\xi} W'(\phi) \right] - 2\rho_w(\phi - 1) \\ &\quad \times U_{\text{vdW}} + \frac{\varepsilon'(\phi)}{2} |\nabla \psi|^2 + 2(\phi - 1)V(\psi), \quad (2.12) \\ -\nabla \cdot \varepsilon(\phi) \nabla \psi_{\text{reac}} + (\phi - 1)^2 V'(\psi_{\text{reac}} + \psi_{\text{vac}}) \\ &= \nabla \cdot [\varepsilon(\phi) - \varepsilon_p \varepsilon_0] \nabla \psi_{\text{vac}}, \quad (2.13) \end{aligned}$$

where $\psi = \psi_{\text{reac}} + \psi_{\text{vac}}$, together with the boundary conditions $\phi = 0$ and $\psi = \psi_\infty$ on $\partial\Omega$, and the initial condition $\phi(\mathbf{x}, 0) = \phi_0(\mathbf{x})$ for all $\mathbf{x} \in \Omega$ for some given function $\phi_0 = \phi_0(\mathbf{x})$. To speed up our computations, we shall first relax the total solvation free energy with CFA (2.8) before switching to the PB free energy. Relaxing the solvation free-energy functional with CFA amounts to solving only the phase-field equation

$$\begin{aligned} \partial_t \phi &= -2P\phi + \gamma_0 \left[\xi \Delta\phi - \frac{1}{\xi} W'(\phi) \right] \\ &\quad - 2(\phi - 1)(\rho_w U_{\text{vdW}} + U_{\text{CFA}}), \end{aligned} \quad (2.14)$$

where U_{CFA} is defined in (2.9).

C. Potential of mean force

We now consider the solvation of two solute objects (e.g., a protein and a ligand) and the effective, solvent-mediated interaction of these two objects by the potential of mean force (PMF) with respect to certain reaction coordinate and reference state. Let us assume that the two solute objects consist of N_1 and N_2 atoms, with $N_1 + N_2 = N$ the total number of solute atoms, located at $\mathbf{x}_1, \dots, \mathbf{x}_{N_1}$ and $\mathbf{x}_{N_1+1}, \dots, \mathbf{x}_N$, respectively. We also assume that the relative positions of all atoms in the same object are fixed. We choose the reaction coordinate d between these two solutes to be the distance between their geometrical centers $(\sum_{i=1}^{N_1} \mathbf{x}_i)/N_1$ and $(\sum_{i=N_1+1}^N \mathbf{x}_i)/(N - N_1)$. We also choose the reference state to be that with $d = d_{\text{ref}} = \infty$, i.e., the two solutes are at infinite separation.

For a finite coordinate d , let us denote by ϕ_d a corresponding free-energy minimizing phase field. We define the (total) PMF as the sum of its separate contributions^{67,82}

$$G_{\text{tot}, \xi}^{\text{PMF}}(d) = G_{\text{geom}, \xi}^{\text{PMF}}(d) + G_{\text{vdW}}^{\text{PMF}}(d) + G_{\text{elec}}^{\text{PMF}}(d),$$

with

$$\begin{aligned} G_{\text{geom}, \xi}^{\text{PMF}}(d) &= F_{\text{geom}, \xi}[\phi_d] - F_{\text{geom}, \xi}[\phi_\infty], \\ G_{\text{vdW}}^{\text{PMF}}(d) &= F_{\text{vdW}}[\phi_d] - F_{\text{vdW}}[\phi_\infty] \\ &\quad + \sum_{i=1}^{N_1} \sum_{j=N_1+1}^N U_{\text{LJ}}^{(i,j)}(|\mathbf{x}_i - \mathbf{x}_j|), \\ G_{\text{elec}}^{\text{PMF}}(d) &= F_{\text{elec}}[\phi_d] - F_{\text{elec}}[\phi_\infty] \\ &\quad + \frac{1}{4\pi \varepsilon_p \varepsilon_0} \sum_{i=1}^{N_1} \sum_{j=N_1+1}^N \frac{Q_i Q_j}{|\mathbf{x}_i - \mathbf{x}_j|}, \end{aligned}$$

where a quantity at ∞ is understood as the limit of that quantity at a coordinate d' as $d' \rightarrow \infty$, and where $U_{\text{LJ}}^{(i,j)}$ is the LJ potential of interaction of solute atoms at \mathbf{x}_i and \mathbf{x}_j , respectively. Any free energy (total or a component) at ∞ can be computed as the sum of the corresponding individual free energies for the two solute objects, respectively. Note for a small reaction coordinate d that the solute-solute vdW interaction, defined by the double sum of $U_{\text{LJ}}^{(i,j)}(|\mathbf{x}_i - \mathbf{x}_j|)$, can be very large, dominating over all other parts in the total PMF. Therefore, in order to better understand the solvent influence in the PMF for small d , it is reasonable to look only at the PMF that excludes the solute-solute vdW interaction.

We remark that, for a given reaction coordinate d , there can be multiple, stable equilibrium phase fields ϕ_d that are different local minimizers of solvation free-energy functional (2.1). Such local minimizers describe different hydration states, such as dry and wet states. Their different solvation free-energy values define different branches of the PMF along the reaction coordinate d and can lead to hysteresis.^{63,65–67,82} Strictly speaking, each of the branches is not a PMF; and the true PMF should be the Boltzmann average of all such branches.

D. Radially symmetric system of a single particle

We now consider the solvation of a single, charged particle (e.g., an ion) by placing a point charge Q at the origin immersed in an aqueous solvent. This corresponds to the case $N = 1$, $\mathbf{x}_1 = O$ (the origin), $\sigma = \sigma_1$, and $\varepsilon = \varepsilon_1$. By the radial symmetry, we assume now the system region is $\Omega = \{\mathbf{x} \in \mathbb{R}^3 : r = |\mathbf{x}| < R_\infty\}$ for some large $R_\infty > 0$, and that both the phase field $\phi = \phi(r)$ and the electrostatic potential $\psi = \psi(r)$ only depend on $r = |\mathbf{x}|$. The phase-field, solvation free-energy functional is now

$$\begin{aligned} F_\xi[\phi] &= 4\pi P \int_0^{R_\infty} [\phi(r)]^2 r^2 dr + 4\pi\gamma_0 \\ &\quad \times \int_0^{R_\infty} \left[\frac{\xi}{2} |\phi'(r)|^2 + \frac{1}{\xi} W(\phi(r)) \right] r^2 dr \\ &\quad + 4\pi\rho_w \int_0^{R_\infty} [\phi(r) - 1]^2 U_{\text{vdW}} r^2 dr \\ &\quad + \frac{1}{2} Q \psi_{\text{reac},\phi}(0) + 4\pi \int_0^{R_\infty} [\phi(r) - 1]^2 \\ &\quad \times \left[\frac{1}{2} \psi_\phi(r) V'(\psi_\phi(r)) - V(\psi_\phi(r)) \right] r^2 dr, \end{aligned} \quad (2.15)$$

where $\psi_\phi = \psi_\phi(r)$ is the electrostatic potential that depends on ϕ . The corresponding reaction field $\psi_{\text{reac},\phi} = \psi_\phi - \psi_{\text{vac}}$ solves PB equation (2.4), which is now

$$\begin{aligned} -\frac{d}{dr} \left[\varepsilon(\phi) r^2 \frac{d\psi_{\text{reac},\phi}}{dr} \right] + r^2 (\phi - 1)^2 V'(\psi_{\text{reac},\phi} + \psi_{\text{vac}}) \\ = -\frac{Q}{4\pi\varepsilon_p\varepsilon_0} \frac{d}{dr} (\varepsilon(\phi)), \end{aligned} \quad (2.16)$$

where we assumed that $\phi = 1$ near $r = 0$. Since ϕ and ψ_ϕ depend only on r , we can convert the integral in (2.11) to obtain the corresponding relaxation dynamics for $\phi = \phi(r, t)$

and $\psi_\phi = \psi_\phi(r, t)$,

$$\begin{aligned} \partial_t \phi &= -2P\phi + \gamma_0 \left[\frac{\xi}{r^2} \frac{d}{dr} \left(r^2 \frac{d\phi}{dr} \right) - \frac{1}{\xi} W'(\phi) \right] \\ &\quad - 2\rho_w (\phi - 1) U_{\text{vdW}} + \frac{\varepsilon'(\phi)}{2} \left(\frac{d\psi_\phi}{dr} \right)^2 \\ &\quad + 2(\phi - 1) V(\psi_\phi), \end{aligned} \quad (2.17)$$

where we absorbed the factor 4π by rescaling the relaxation time variable t , together with PB equation (2.16) for each time t . We use the boundary conditions $\phi(0) = 1$, $\phi(R_\infty) = 0$, $\psi'_{\text{reac},\phi}(0) = 0$, and $\psi_{\text{reac},\phi}(R_\infty) = \psi_\infty - \psi_{\text{vac}}(R_\infty)$, where ψ_∞ is now a given constant. We often choose

$$\psi_\infty = \frac{Qe^{-\kappa(R_\infty - R_0)}}{4\pi\varepsilon_w\varepsilon_0(1 + \kappa R_0)R_\infty},$$

which is the value at R_∞ of the Debye–Hückel potential (analytical solution to the linearized PB equation) for a sphere of radius R_0 with point charge Q at center immersed in the ionic solution with κ being the inverse Debye length. We estimate R_0 to be close to the LJ parameter σ . We choose our initial phase field $\phi_0 = \phi_0(r)$ to be

$$\phi_0(r) = \frac{1}{2} + \frac{1}{2} \tanh \left(\frac{R_0 - r}{\xi/3} \right).$$

If we apply the linearized PB equation, then the last integral in $F_\xi[\phi]$ in (2.15) vanishes. Moreover, we can compare with the sharp-interface formulation in which a possible dielectric boundary is determined by the radius R of the spherically charged particle, and the solvation free energy becomes⁶⁷

$$\begin{aligned} G[R] &= \frac{4}{3}\pi P R^3 + 4\pi\gamma_0 R^2 + 16\pi\rho_w\varepsilon \left(\frac{\sigma^{12}}{9R^9} - \frac{\sigma^6}{3R^3} \right) \\ &\quad + \frac{Q^2}{8\pi\varepsilon_0 R} \left[\frac{1}{\varepsilon_w(1 + \kappa R)} - \frac{1}{\varepsilon_p} \right]. \end{aligned} \quad (2.18)$$

This simple one-dimensional function can be minimized numerically with a very high accuracy. The optimal R can be used as our R_0 in ψ_∞ and $\phi_0(r)$.

In the case that $\kappa = 0$, i.e., the ionic effect is very small and can be neglected, we can solve Poisson's equation (2.16) together with the boundary condition that $\psi'_{\text{reac},\phi}(0) = 0$ to obtain

$$r^2 \psi'_{\text{reac},\phi}(r) = \frac{Q}{4\pi} \left(\frac{1}{\varepsilon(1)} - \frac{1}{\varepsilon(\phi)} \right). \quad (2.19)$$

This implies that $r^2 \psi'_\phi(r) = -Q/(4\pi\varepsilon(\phi(r)))$, where the value at $r = 0$ is understood as the limit as $r \rightarrow 0$. This limit exists and is the same as $\lim_{r \rightarrow 0} r^2 \psi'_{\text{vac}}(r) = -Q/(4\pi\varepsilon_p\varepsilon_0)$. Consequently, since $V = 0$ in this case, Eq. (2.17) becomes

$$\begin{aligned} \partial_t \phi &= -2P\phi + \gamma_0 \left[\frac{\xi}{r^2} \frac{d}{dr} \left(r^2 \frac{d\phi}{dr} \right) - \frac{1}{\xi} W'(\phi) \right] \\ &\quad - 2\rho_w (\phi - 1) U_{\text{vdW}} + \frac{Q^2 \varepsilon'(\phi)}{32\pi^2 (\varepsilon(\phi))^2 r^4}, \end{aligned} \quad (2.20)$$

where we used the fact that $\phi(r) = 1$, and hence $\varepsilon'(\phi(r)) = 0$, for r near 0. Note in this case that we do not need to solve any equation for the electrostatic potential. Once we obtain a stable equilibrium phase-field ϕ , we can obtain by (2.19) and

the boundary condition $\psi_\phi(R_\infty) = Q/(4\pi\varepsilon_w\varepsilon_0)$ that

$$\psi_{\text{reac},\phi}(r) = \frac{Q}{4\pi R_\infty} \left(\frac{1}{\varepsilon_w\varepsilon_0} - \frac{1}{\varepsilon_p\varepsilon_0} \right) + \int_r^{R_\infty} \frac{Q}{4\pi s^2} \left[\frac{1}{\varepsilon(\phi(s))} - \frac{1}{\varepsilon_p\varepsilon_0} \right] ds.$$

Finally, the electrostatic energy is

$$F_{\text{cle}}[\phi] = \frac{1}{2}Q\psi_{\text{reac},\phi}(0) = \frac{Q^2}{8\pi R_\infty} \left(\frac{1}{\varepsilon_w\varepsilon_0} - \frac{1}{\varepsilon_p\varepsilon_0} \right) + \int_0^{R_\infty} \frac{Q^2}{8\pi s^2} \left[\frac{1}{\varepsilon(\phi(s))} - \frac{1}{\varepsilon_p\varepsilon_0} \right] ds, \quad (2.21)$$

where we note that $\phi(s) = 1$ near $s = 0$. If R_0 is the optimal, sharp, dielectric boundary defined by $\phi(R_0) = 1/2$, and we replace $\phi(s)$ by its sharp-interface version, $\phi(s) = 1$ for $s < R_0$ and $\phi(s) = 0$ for $s > R_0$, then we obtain exactly the Born energy

$$F_{\text{cle}}[\phi] = \frac{1}{2}Q\psi_{\text{reac},\phi}(0) = \frac{Q^2}{8\pi R_0} \left(\frac{1}{\varepsilon_w\varepsilon_0} - \frac{1}{\varepsilon_p\varepsilon_0} \right).$$

III. NUMERICAL METHODS

A. Discretization and algorithm

We choose some $L > 0$ and set $\Omega = (-L, L)^3$. We choose a positive integer Ng and cover Ω by a uniform grid with $Ng \times Ng \times Ng$ grid cells. All the grid points are labeled by (i, j, k) . We also choose a time step $\Delta t > 0$ and set $t_n = n\Delta t$ for $n = 1, 2, \dots$. For a given function $u = u(\mathbf{x}, t)$, we denote by $u^{(n)}(\mathbf{x})$ and $u_{i,j,k}^{(n)}$ approximations of $u(\mathbf{x}, t_n)$ and $u(\mathbf{x}_{i,j,k}, t_n)$, respectively.

Given $\phi^{(n)}$ and $\psi^{(n)}$, hence also $\psi_{\text{reac}}^{(n)} = \psi^{(n)} - \psi_{\text{vac}}$. We approximate the left-hand side $\partial_t\phi$ of Eq. (2.12) by $(\phi^{(n+1)} - \phi^{(n)})/\Delta t$. We approximate ϕ by $\phi^{(n+1)}$ in $-2P\phi$ and $\gamma_0\Delta\phi$ and approximate ϕ and ψ by $\phi^{(n)}$ and $\psi^{(n)}$ in all the other terms on the right-hand side of (2.12). Once we get $\phi^{(n+1)}$, we use it to replace ϕ in PB equation (2.13) for solving for $\psi^{(n+1)}$. After working out details, we obtain the following semi-implicit scheme:

$$(1 + 2P\Delta t)\phi^{(n+1)} - \gamma_0\xi\Delta t\Delta\phi^{(n+1)} = \phi^{(n)} + \Delta t \left[-\frac{\gamma_0}{\xi}W'(\phi^{(n)}) - 2\rho_w(\phi^{(n)} - 1)U_{\text{vdW}} + \frac{\varepsilon'(\phi^{(n)})}{2}|\nabla\psi^{(n)}|^2 + 2(\phi^{(n)} - 1)V(\psi^{(n)}) \right], \quad (3.1)$$

$$-\nabla \cdot \varepsilon(\phi^{(n+1)})\nabla\psi_{\text{reac}}^{(n+1)} + (\phi^{(n+1)} - 1)^2V'(\psi_{\text{reac}}^{(n+1)} + \psi_{\text{vac}}) = \nabla \cdot [\varepsilon(\phi^{(n+1)}) - \varepsilon_p\varepsilon_0]\nabla\psi_{\text{vac}}. \quad (3.2)$$

These, together with the boundary conditions $\phi^{(n+1)} = 0$ and $\psi_{\text{reac}}^{(n+1)} = \psi_\infty - \psi_{\text{vac}}$ on $\partial\Omega$, determine uniquely $\phi^{(n+1)}$ and $\psi_{\text{reac}}^{(n+1)}$. For the nonlinear PB equation, we can use Newton's iteration with linearization around $\psi^{(n)}$ to solve (3.2). We use the central difference scheme for spatial discretization of $\Delta\phi$ and $\nabla \cdot \varepsilon(\phi)\nabla\psi$. The coefficient matrices of the resulting linear systems are symmetric positive definite. We use the conjugate gradient method or multigrid method to solve these systems of equations. To speed up our computations, we shall first use

CFA and then switch to the PB equation. In a similar way, we can discretize equation (2.14) to obtain

$$(1 + 2P\Delta t)\phi^{(n+1)} - \gamma_0\xi\Delta t\Delta\phi^{n+1} = \phi^{(n)} + \Delta t \left[-\frac{\gamma_0}{\xi}W'(\phi^{(n)}) - 2(\phi^{(n)} - 1) \times (\rho_wU_{\text{vdW}} + U_{\text{CFA}}) \right]. \quad (3.3)$$

Note that we choose some $\zeta \in (0, 0.5)$ and after we solve Eq. (3.1) or (3.3), set $\phi^{(n+1)} = 1$ at any grid point that is inside any ball $B(\mathbf{x}_i, \sigma_{i,\text{cut}})$ with $\sigma_{i,\text{cut}} = \max\{1, \zeta\sigma_i\}$ for each i ($1 \leq i \leq N$).

We use two different types of initial phase fields $\phi^{(0)} = \phi^{(0)}(\mathbf{x})$. One is a tight wrap. It corresponds to a molecular surface. The other is a loose wrap that corresponds to a large surface (e.g., a sphere) that encloses all the solute atoms. Practically, we use

$$\phi^{(0)}(\mathbf{x}) = \tanh\left(\frac{1}{\xi}\text{dist}(\mathbf{x}, \cup_{i=1}^N B(\mathbf{x}_i, r_i))\right),$$

where $B(\mathbf{x}_i, r_i)$ is the ball of radius r_i centered at \mathbf{x}_i and all r_i are adjustable parameters and modify $\phi^{(0)}$ so that it takes the value 1 close to any \mathbf{x}_i ($1 \leq i \leq N$).

Algorithm

- Step 1. Input all the parameters. Set the geometrical center of $\mathbf{x}_1, \dots, \mathbf{x}_N$ to be the origin. Define a uniform grid covering $\Omega = (-L, L)^3$ and choose a time step Δt . Compute $U_{\text{vdW}}(\mathbf{x}_{i,j,k})$ and $U_{\text{CFA}}(\mathbf{x}_{i,j,k})$ at all the grid points $\mathbf{x}_{i,j,k}$ that are not locations of any solute atoms. Choose $\zeta \in (0, 0.5)$. Generate an initial phase field $\phi^{(0)}$.
- Step 2. Choose an integer N_{CFA} . For $n = 0, \dots, N_{\text{CFA}}$, solve Eq. (3.3) with the boundary conditions $\phi^{(n+1)} = 0$ on $\partial\Omega$. Set $\phi^{(n+1)} = 1$ at grid points that have distance to \mathbf{x}_i smaller than $\max\{1, \zeta\sigma_i\}$ ($1 \leq i \leq N$). Set $n = 0$ and $\phi^{(0)} = \phi^{(N_{\text{CFA}}+1)}$ and choose an error tolerance parameter ε_{tor} .
- Step 3. Solve Eq. (3.1) with the boundary condition $\phi^{(n+1)} = 0$ on $\partial\Omega$. Set $\phi^{(n+1)} = 1$ at grid points that have distance to \mathbf{x}_i smaller than $\max\{1, \zeta\sigma_i\}$ ($1 \leq i \leq N$). Then solve PB equation (2.13) with the boundary condition $\psi^{(n+1)} = \psi_\infty$ on $\partial\Omega$. If

$$\|\phi^{(n+1)} - \phi^{(n)}\|_{L^2(\Omega)} + \|\psi_{\text{reac}}^{(n+1)} - \psi_{\text{reac}}^{(n)}\|_{L^2(\Omega)} \leq \varepsilon_{\text{tor}},$$

then stop. Otherwise, set $n := n + 1$ and repeat this step.

- Step 4. Let ϕ and ψ be the solutions from last step. Compute the free energy $F_\xi[\phi]$. Set $\{\mathbf{x} \in \Omega : \phi(\mathbf{x}) = 1/2\}$ as the equilibrium solute-solvent interface.

B. Convergence test

We first test our code for solving Equations (2.12) and (2.13). They are both of the type

$$-\nabla \cdot a\nabla u + bu = f \quad \text{in } \Omega, \quad (3.4)$$

$$u = u_\infty \quad \text{on } \partial\Omega, \quad (3.5)$$

where $a = a(\mathbf{x})$, $b = b(\mathbf{x})$, $f = f(\mathbf{x})$, and $u_\infty = u_\infty(\mathbf{x})$ are smooth and bounded functions, and a is bounded below by

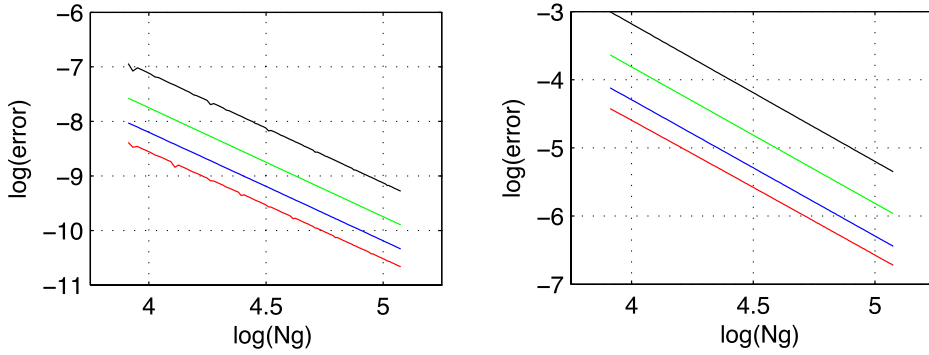


FIG. 3. The log-log plot of the absolute error in different norms vs. the number of grid points N_g in one direction for the first (left) and second (right) cases. Red (bottom) line: Absolute error in L^1 -norm. Blue (second to the bottom) line: Absolute error in L^2 -norm of the error. Black (top) line: Absolute error in L^∞ -norm. Green line (second line from top): line of slope 2 for comparison. A second-order convergence rate is observed for both cases.

a positive constant and b is nonnegative. We set $\Omega = (-5, 5) \times (-5, 5) \times (-5, 5)$ and consider two cases. In the first case, we mimic the coefficients in ϕ -equation (2.12) and set $a = 0.001$, $b = 1$, $u_\infty = 0$, and f is obtained by (3.4) with the exact solution

$$u(x, y, z) = \sin(\pi x) \sin(\pi y) \sin(\pi z).$$

In the second case, we set $a(x, y, z) = 80 + 70 \sin(x + y + z)$, $b = (\eta - 1)^2$ with $\eta(x, y, z) = \sin(\pi x/10) \sin(\pi y/10) \sin(\pi z/10)$, and f and u_∞ by (3.4) and (3.5) with the exact solution

$$u(x, y, z) = \sin\left(\frac{\pi x}{10}\right) \sin\left(\frac{\pi y}{10}\right) \sin\left(\frac{\pi z}{10}\right) + x^2 + (y - 1)(z + 3).$$

We discretize these equations using central finite difference schemes and solve the resulting systems of equations using a preconditioned conjugate gradient method. For each of the two cases, we use a grid of $N_g \times N_g \times N_g$ grid points with $N_g \in \{50, 51, \dots, 147, 148\}$. In Fig. 3, we plot in the log-log scale the absolute errors of our numerical solutions in different norms vs. the number of grid points N_g in one direction. We see that our numerical method achieves a second-order convergence rate as expected.

We now test our model and algorithm for a spherical particle with a point charge Q at center immersed in an ionic solution to demonstrate that our phase-field model “converges” to the corresponding sharp-interface model as the numeri-

TABLE I. A comparison of numerical results obtained by minimizing the phase-field solvation free-energy functional $F_\xi[\phi]$ defined in (2.15) and the sharp-interface solvation free-energy functional $G = G[R]$ defined in (2.18) for the radially symmetric one-particle system. The sharp-interface results are presented in the last column. See the text for the units.

Q	Optimal radius/energy	$\xi = 0.1$	$\xi = 0.05$	$\xi = 0.02$	$\xi = 0.01$	$\xi = 0.005$	Sharp interface
0.0	R_{\min}	3.039	3.043	3.047	3.047	3.047	3.054
	F_{surf}	20.313	20.361	20.412	20.414	20.407	20.511
	F_{vdW}	-2.653	-2.603	-2.589	-2.569	-2.556	-2.644
	F_{elec}	0.000	0.000	0.000	0.000	0.000	0.000
	F_{tot}	17.660	17.759	17.823	17.845	17.851	17.867
0.5	R_{\min}	2.953	2.958	2.960	2.960	2.960	2.961
	F_{surf}	19.189	19.247	19.269	19.266	19.266	19.275
	F_{vdW}	-1.245	-1.189	-1.127	-1.090	-1.073	-1.067
	F_{elec}	-23.356	123.270	-23.242	-23.241	-23.241	-23.236
	F_{tot}	-5.412	-5.212	-5.100	-5.066	-5.015	-5.028
1.0	R_{\min}	2.755	2.766	2.772	2.771	2.771	2.772
	F_{surf}	16.789	16.869	16.858	16.697	16.881	16.902
	F_{vdW}	4.978	4.882	4.900	4.998	5.067	5.048
	F_{elec}	-100.154	-99.525	-99.299	-99.302	-99.289	-99.238
	F_{tot}	-78.387	-77.774	-77.541	-77.607	-77.340	-77.288
1.5	R_{\min}	2.561	2.581	2.593	2.592	2.593	2.594
	F_{surf}	15.089	14.902	14.825	14.648	14.795	14.800
	F_{vdW}	18.615	17.854	17.465	17.729	17.848	17.806
	F_{elec}	-242.564	-239.969	-238.817	-238.826	-238.740	-238.586
	F_{tot}	-208.860	-207.213	-206.528	-206.449	-206.097	-205.980
2.0	R_{\min}	2.386	2.425	2.448	2.449	2.448	2.446
	F_{surf}	17.673	14.089	13.480	13.197	13.255	13.195
	F_{vdW}	42.473	39.522	37.503	37.994	38.444	38.449
	F_{elec}	-465.014	-454.035	-449.668	-449.503	-449.464	-449.152
	F_{tot}	-404.867	-400.424	-398.685	-398.311	-397.765	-397.506

TABLE II. Hydration free energies in $k_B T$ for single ions K^+ , Na^+ , Cl^- , and F^- obtained by PF-VISM and by experiment. The second column lists experimental values of hydration free energies for these ions, with E_{spec} from Ref. 107 and E_{ave} averaged from dozens of data sets collected in Ref. 104. The third column lists two different sets of the LJ parameters ε and σ for each ion, with $\varepsilon_{\text{spec}}$, σ_{spec} designed in Ref. 106 and ε_{ave} , σ_{ave} averaged over a few sets of data collected in Ref. 106. The fourth column is the amount of shift in the dielectric profile of $\varepsilon = \varepsilon(\phi)$, cf. Eqs. (2.6) and (2.7) and Fig. 2. Numbers in the last three columns are our numerical values of the hydration free energies for different numerical values of ξ .

Ions	Experiment	ε and σ	Shift	PF-VISM		
				$\xi = 0.5$	$\xi = 0.1$	$\xi = 0.05$
K^+	$E_{\text{spec}} = -117.51$	$\varepsilon_{\text{spec}} = 0.008$	0	-148.86	-137.58	-129.29
		$\sigma_{\text{spec}} = 3.850$	1/3	-165.66	-157.03	-149.08
	$E_{\text{ave}} = -133.72$	$\varepsilon_{\text{ave}} = 0.201$	0	-121.10	-108.26	-98.17
		$\sigma_{\text{ave}} = 3.403$	1/3	-134.53	-123.76	-116.06
Na^+	$E_{\text{spec}} = -145.39$	$\varepsilon_{\text{spec}} = 0.008$	0	-175.55	-165.22	-159.40
		$\sigma_{\text{spec}} = 3.49$	1/3	-194.98	-188.09	-182.25
	$E_{\text{ave}} = -160.25$	$\varepsilon_{\text{ave}} = 0.182$	0	-150.29	-140.17	-131.67
		$\sigma_{\text{ave}} = 2.998$	1/3	-166.55	-158.73	-152.07
Cl^-	$E_{\text{spec}} = -135.43$	$\varepsilon_{\text{spec}} = 0.207$	0	-100.74	-85.56	-81.36
		$\sigma_{\text{spec}} = 3.780$	1/3	-112.28	-100.26	-81.54
	$E_{\text{ave}} = -125.32$	$\varepsilon_{\text{ave}} = 0.245$	0	-99.29	-81.75	-80.83
		$\sigma_{\text{ave}} = 3.780$	1/3	-110.54	-98.40	-81.00
F^-	$E_{\text{spec}} = -185.22$	$\varepsilon_{\text{spec}} = 0.219$	0	-126.23	-113.75	-103.90
		$\sigma_{\text{spec}} = 3.30$	1/3	-139.85	-130.34	-122.35
	$E_{\text{ave}} = -174.50$	$\varepsilon_{\text{ave}} = 0.232$	0	-122.33	-109.69	-99.67
		$\sigma_{\text{ave}} = 3.348$	1/3	-135.77	-125.96	-177.73

cal parameter $\xi \rightarrow 0$. We choose $\xi = 0.1, 0.05, 0.02, 0.01$, and 0.005 in the unit \AA and $Q = 0.0, 0.5, 1.0, 1.5$, and 2.0 in the unit of elementary charge e . For each of these values Q and ξ , we minimize the solvation free-energy functional $F_\xi[\phi]$ defined in (2.15) with the linearized PB electrostatics and obtain the optimal radius R_{min} , the minimum total free energy F_{tot} , and all the corresponding components of the free energy: the surface energy F_{surf} , the solute-solvent vdW energy F_{vdW} , and the electrostatic energy F_{ele} . The minimization is done by solving Equations (2.17) and (2.16) with the corresponding initial solution for ϕ and boundary conditions for both ϕ and ψ_ϕ . The sharp-interface solvation free-energy functional with the linearized PB electrostatics is given as a one-variable function $G = G[R]$ defined in (2.18). We minimize it numerically and obtain the optimal radius, total free energy, and all the components of the free energy. We use the following parameters: the pressure difference $P = 0$ bar, effective surface tension

$\gamma_0 = 0.175 k_B T / \text{\AA}^2$, solvent bulk density $\rho_w = 0.0333 \text{\AA}^{-3}$, LJ parameters $\varepsilon = 0.3 k_B T$ and $\sigma = 3.5 \text{\AA}$, dielectric coefficients $\varepsilon_p = 1$ and $\varepsilon_w = 80$, and the inverse Debye length $\kappa = 0.1 \text{\AA}^{-1}$. (For the case $Q = 0 e$, we set $\kappa = 0 \text{\AA}^{-1}$.) We summarize our test results in Table I. It is clear that as ξ becomes smaller and smaller, the corresponding optimal radii and total free energies are closer and closer to those of the sharp-interface model.

IV. RESULTS

A. Single ions: Solvation free energy and dielectric boundary

We use our PF-VISM to calculate the hydration free energies for single ions K^+ , Na^+ , Cl^- , and F^- in water and compare our results with experimental data. We shall show how the

TABLE III. PF-VISM hydration free energies in $k_B T$ for the anions Cl^- and F^- with the new LJ parameters $\varepsilon_{\text{new}} = \varepsilon_{\text{ave}} k_B T$ and $\sigma_{\text{new}} = \sigma_{\text{ave}} - 0.5 \text{\AA}$, with comparison with experiment. All the other parameters and data are the same as in Table II.

Ions	Experiment	ε and σ	Shift	PF-VISM		
				$\xi = 0.5$	$\xi = 0.1$	$\xi = 0.05$
Cl^-	$E_{\text{spec}} = -135.43$	$\varepsilon_{\text{new}} = 0.245$	0	-128.45	-116.41	-106.72
	$E_{\text{ave}} = -125.32$	$\sigma_{\text{new}} = 3.280$	1/3	-142.46	-133.16	-125.33
F^-	$E_{\text{spec}} = -185.22$	$\varepsilon_{\text{new}} = 0.232$	0	-156.00	-148.23	-140.18
	$E_{\text{ave}} = -174.50$	$\sigma_{\text{new}} = 2.848$	1/3	-171.79	-167.21	-160.93

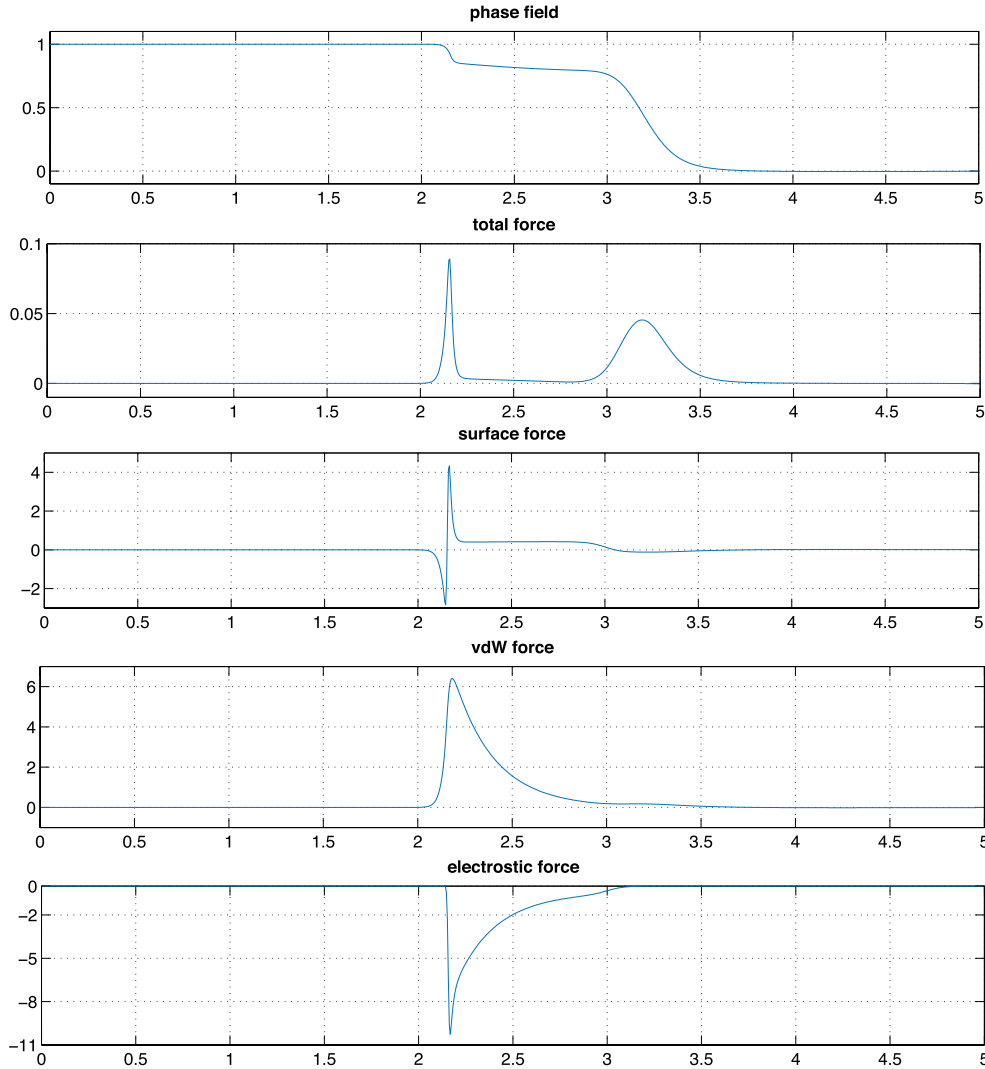


FIG. 4. A typical plot of the phase field, total force, and different force components. The horizontal axis is the radial axis r . From top to bottom: an equilibrium phase field; the total force; the surface force; the vdW force; and the electrostatic force. Two different boundaries can be seen clearly in the interfacial region.

interplay between the ionic geometry, vdW dispersive force, and the charge effect can contribute to the hydration free energy of a single ion through a few adjustable parameters. We shall also show how the flexibility of a diffuse interface can possibly describe microscopic properties in the solute-solvent interfacial layer, particularly boundary locations for different kinds of interfaces. Experimental data are used here more as guidelines, as such data are very dispersive.¹⁰⁴

For all of these ions, we use the following parameters and data: $T = 298$ K; $P = 0$ bar; $\gamma_0 = 0.06 k_B T / \text{\AA}^2$; (this is calculated using the curvature correction $1 - 2\delta/R$ to the usual planar surface tension value $0.175 k_B T / \text{\AA}^2$ with the Tolman length $\delta \approx 1$ \AA and with the ionic radius $R \approx 3$ \AA) $\rho_w = 0.0333 \text{\AA}^{-3}$; $Q = 1 e$ (elementary charge) for K^+ and Na^+ and $Q = -1 e$ for Cl^- and F^- ; $\epsilon_0 = 1.41765 \times 10^{-4} e^2 (k_B T)^{-1} \text{\AA}^{-1}$; $\epsilon_p = 1$; $\epsilon_w = 80$; $\kappa = 0$ \AA; (this approximation results from our assumption that there are no other ions nearby in the system) and $\xi = 0.5, 0.1, 0.05$ \AA. We use two sets of ion-water LJ parameters ϵ in $k_B T$ and σ in \AA. One is averaged from 4–8 data sets collected in Ref. 106 and will be denoted by ϵ_{ave} and σ_{ave} . The other is optimally designed in the same work¹⁰⁶ and will be denoted by ϵ_{spec} and σ_{spec} . We converted the units of energy

to $k_B T$. We compare two sets of experimental values of ionic hydration free energies in $k_B T$. One is averaged from a few dozens of data collected in Ref. 104 and will be marked as E_{ave} . The other is from Ref. 107 and will be marked E_{spec} . We converted the units to $k_B T$.

Due to the radial symmetry and since $\kappa = 0$, we need only to solve ϕ -equation (2.20) without solving the ψ -equation and evaluate the free energy by (2.21). We choose initially very fine spatial finite difference grid (e.g., the grid size $h = 0.001$), very small time step (e.g., $\Delta t = 0.00001$), and very large number of total time iteration steps (e.g., 10^6 – 10^7). We then reduce largely the number of grid points, increased the time step, and reduced the total number of time iterations. For both sets of these numerical parameters, we obtain almost the same results. In average, we need only a few minutes to half an hour to finish one run. Note that we do not shift our final phase-field dielectric boundary to calculate the electrostatic free energy.

In Table II, we display our PF-VISM calculation results. We observe that overall our PF-VISM predicted hydration free energies agree with experimental data very well, with better results for cations than anions. The best parameters for all the ionic systems are the averaged LJ parameters ϵ_{ave} , σ_{ave} , the

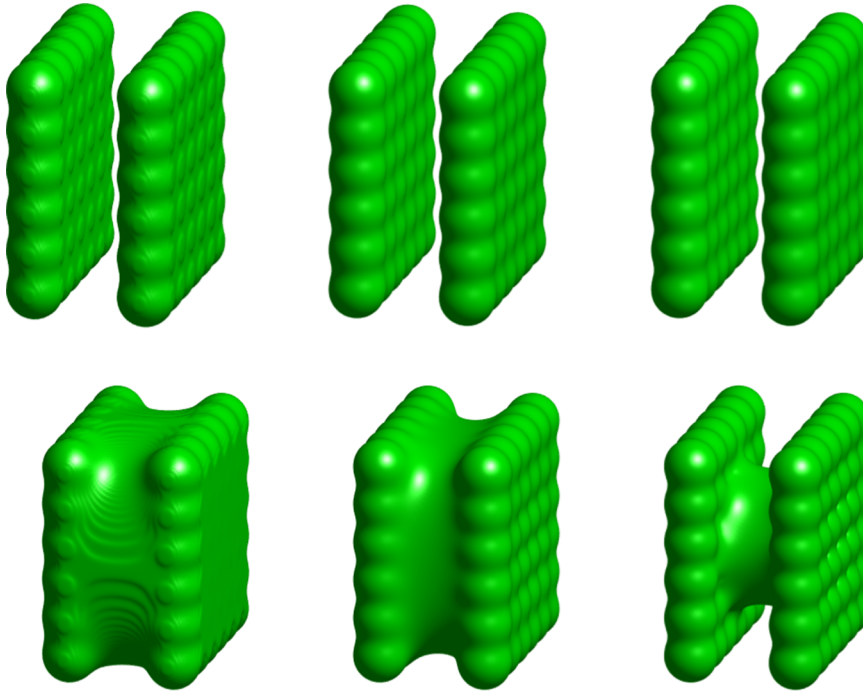


FIG. 5. Solute-solute interfaces of the two-plate system obtained by the PF-VISM computation with the linearized PB electrostatics. In each individual part, a colored region is the solute region without solvent. Outside the colored region is the solvent region. The colored interface is defined as the $1/2$ -level set of a phase-field function $\{\mathbf{x} : \phi(\mathbf{x}, t) = 1/2\}$, where $\phi(\mathbf{x}, t)$ solves Eqs. (2.12) and (2.13) with a tight initial (top) and loose initial (bottom) phase field. The separation distance is $d = 12 \text{ \AA}$. The charges are $(q_1, q_2) = (0 e, 0 e)$ (left), $(q_1, q_2) = (0.1 e, 0.1 e)$ (middle), and $(q_1, q_2) = (-0.1 e, 0.1 e)$ (right).

amount of dielectric shift $1/3$, and the numerical value $\xi = 0.5$. By a more careful check, we find that the 10% reduction of ξ from $\xi = 0.5$ to $\xi = 0.05$ leads to a 10%–5% reduction of the free energy, consistent for all the systems. In a MD forcefield, the ion-water LJ parameter σ for an anion can be in general larger than that for a cation with the same crystal radius, since a water molecule is often considered to be centered near the center of oxygen. Therefore, we introduce the new LJ parameters $\sigma_{\text{new}} = \sigma_{\text{ave}} - 0.5 \text{ \AA}$ and $\varepsilon_{\text{new}} = \varepsilon_{\text{ave}}$ for the anions Cl^- and F^- . With such LJ parameters, we then obtain much better PF-VISM estimates for the hydration free energies for the anions, cf. Table III.

Fig. 4 shows a typical profile of a stable equilibrium phase field ϕ obtained from solving Eq. (2.20), the corresponding total force $-\delta_\phi F_\xi[\phi]$ which is the right-hand side of Eq. (2.20), and the different force components. They are the surface force, vdW force, and electrostatic force corresponding to the second, third, and fourth terms on the right-hand side of Eq. (2.20). It is clear that within the interfacial region there are two boundaries. One of them is where the magnitude of elec-

trostatic force reaches the maximal value and different forces balance.

B. Two charged parallel plates: Potential of mean force

We now consider a system of two parallel solute plates in an aqueous solution. Due to its unique geometrical features, such and similar systems have been used extensively to study the hydrophobic interaction and charge effect.^{41,43,54,55,58,61,65,67,82,108} The specific two-plate system we study here is the same as that studied by MD simulations in Ref. 41 and VISM with CFA in Refs. 61, 67, and 82. Our system setup and results are similar to those in Refs. 67 and 82. Each plate consists of 6×6 fixed CH_2 atoms with the atom-to-atom distance 2.1945 \AA . The plate has a square length of about 30 \AA . We use the following parameters: $P = 0$ bar; $\gamma_0 = 0.175 k_B T / \text{\AA}^2$; $\rho_w = 0.0333 \text{ \AA}^{-3}$; $\varepsilon_p = 1$; $\varepsilon_w = 80$; and $\kappa = 0.1 \text{ \AA}^{-1}$; the solute-solute LJ parameters for each solute atom in the plate $\varepsilon = 0.3 k_B T$ and $\sigma = 3.5 \text{ \AA}$; and

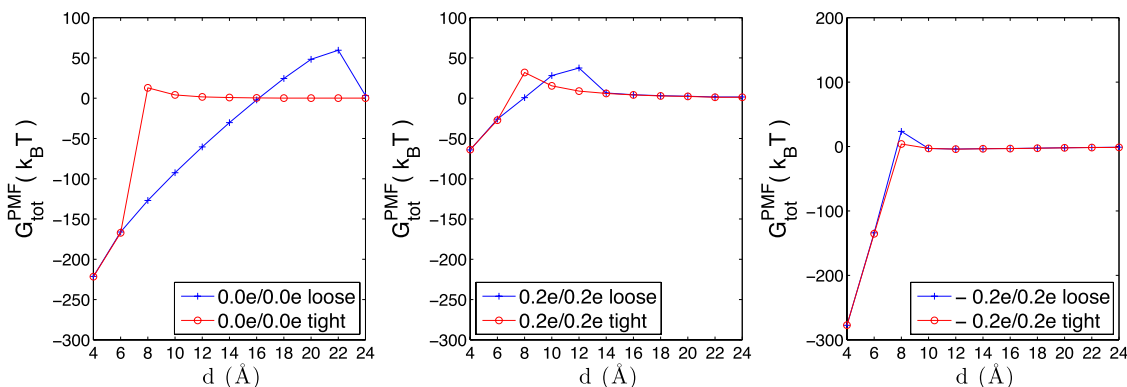


FIG. 6. The two PMF branches corresponding to the wet (red and circles) and dry (blue and +), in certain range of d states for the two plates with different charging patterns.

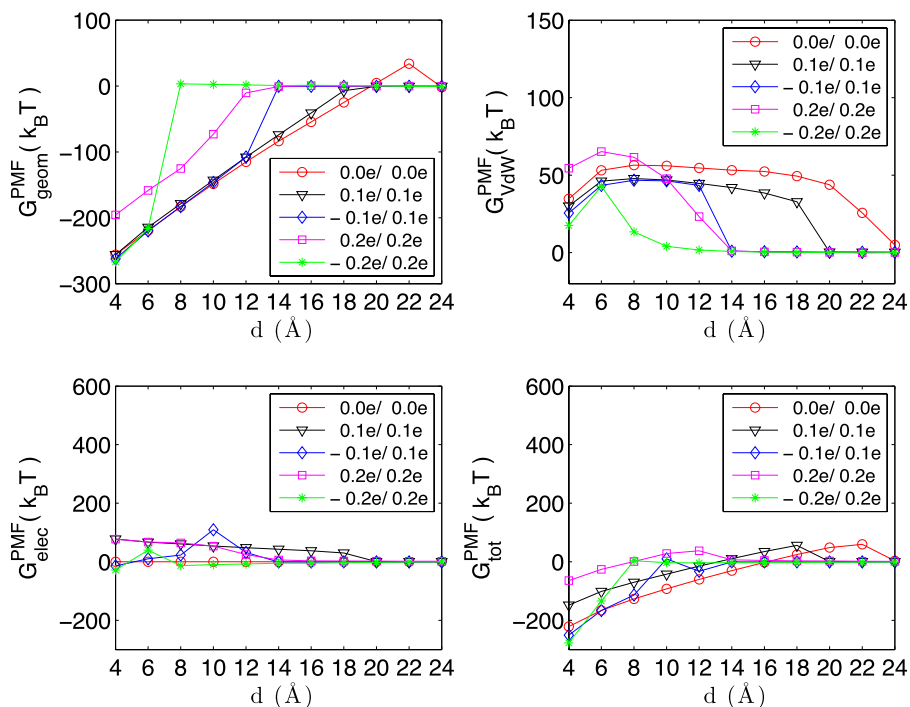


FIG. 7. Different components of the PMF for the two-plate system for different charge combinations (q_1, q_2) (see legend) obtained by the PF-VISM with loose initial surfaces.

$\xi = 1$. We assign the charges q_1 and q_2 to the center of each solute atom in the first and second plates, respectively, with $|q_1| = |q_2|$. The total charges of these two plates are $36q_1$ and $36q_2$, respectively. We choose the values of (q_1, q_2) to be $(0 e, 0 e)$, $(+0.1 e, -0.1 e)$, $(+0.1 e, +0.1 e)$, $(+0.2 e, -0.2 e)$, and $(+0.2 e, +0.2 e)$, respectively. We define the center-to-center distance between these two parallel plates as the reaction coordinate and denote it by d with the unit \AA . For each of a few selected d values, we use two different types of initial phase fields. One is a tight wrap which consists of two surfaces tightly wrapping up the two plates, respectively. The other is a loose wrap, a large box containing both of the plates.

Once an initial phase field is chosen, we solve Eqs. (2.12) and (2.13) on the computational box $\Omega = (-L, L)^3$ with $L = 25 \text{\AA}$ to obtain a steady-state solution which in turn determines a stable equilibrium solute-solvent interface.

In Fig. 5, we display our PF-VISM equilibrium solute-solvent interfaces of the two-plate system with $d = 12 \text{\AA}$, tight initial phase fields (top) and loose initial phase fields (bottom), and the charges $(q_1, q_2) = (0 e, 0 e)$ (left), $(q_1, q_2) = (0.1 e, 0.1 e)$ (middle), and $(q_1, q_2) = (-0.1 e, 0.1 e)$ (right). We see that the PF-VISM equilibrium surfaces obtained with tight initials are all very similar to a molecular surface (i.e., SES). Moreover, it is clear that the PF-VISM with tight and

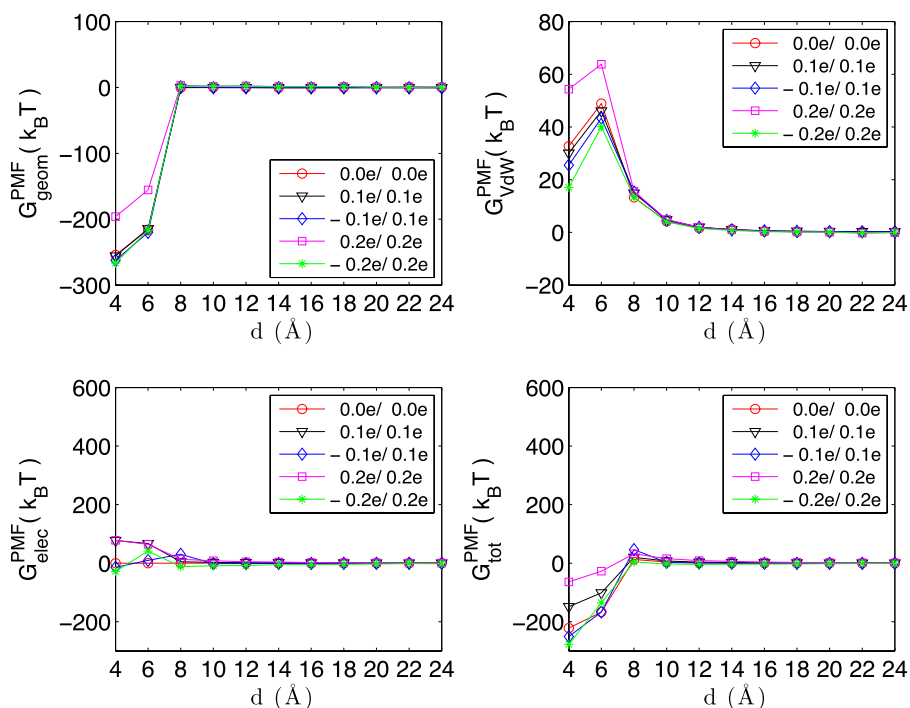


FIG. 8. Different components of the PMF for the two-plate system for different charge combinations (q_1, q_2) (see legend) obtained by the PF-VISM with tight initial surfaces.

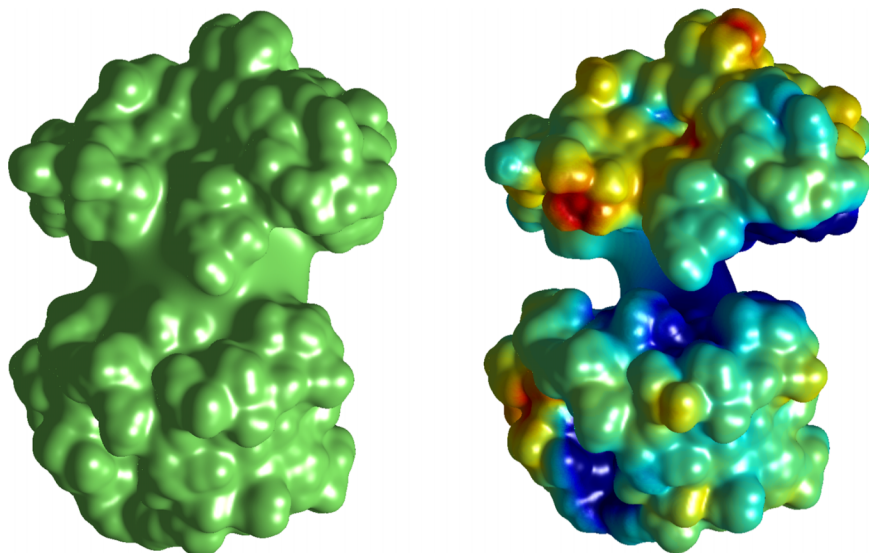


FIG. 9. Conformations of BphC obtained by PF-VISM computation with PB electrostatics. Left: no partial charges. Right: with partial charges. Color on the right image indicates the electrostatic potential distribution: blue for positive and red for negative values.

loose initials predict wet and dry states, respectively, and that the electrostatics wets the inter-plate region, agreeing with MD simulations and previous level-set VISM calculations.^{41,43,61,65,67,82,108} Note that the dielectric boundary force always directs from the high dielectric solvent region to the low dielectric solute region, and the PB based continuum electrostatics theory predicts such a force direction.^{105,109–111} This is the reason that with the solute partial charges, the dielectric boundary is pushed in to wet the system. The asymmetric charges $(q_1, q_2) = (-0.1 e, 0.1 e)$ give rise to a stronger electric field and hence a larger dielectric boundary force. It drags more polar water into the void, and the system (bottom-right) is wetter than that (bottom-middle) with symmetric charges $(q_1, q_2) = (0.1 e, 0.1 e)$.

Fig. 6 shows the two different PMF branches for the two-plate system with several, different values of partial charges. These PMFs exhibit clearly the bimodal behavior and hysteresis of the system. For the neutral plates (cf. Fig. 5, left), a strong hysteresis is present for $6 \lesssim d \lesssim 16 \text{ \AA}$. Adding charges influences the free-energy branches and hysteresis as shown in Fig. 6 (middle and right). The charge effect with oppositely charged plates is most significant as a strong electrostatic field develops in between the hydrophobic plates.

In Figs. 7 and 8, we plot the different components of the PMF with loose and tight initial surfaces, respectively. For the loose initials (Fig. 7), the geometric part (i.e., the surface energy part) displays a strong attraction below a critical distance

d_c at which capillary evaporation begins. This crossover distance decreases from $d_c \approx 22 \text{ \AA}$ for $(q_1, q_2) = (0 e, 0 e)$ down to 8 \AA for $(q_1, q_2) = (-2 e, 2 e)$. The value 22 \AA is larger than 14 \AA predicted by the sharp-interface VISM where the curvature correction was included. Note that the opposite charging has a much stronger effect than like-charging due to the electrostatic field distribution discussed above. Also, the solute-solvent vdW part of the interaction is strongly affected by electrostatics due to the very different surface geometries induced by charging. Both curves $G_{\text{geom}}^{\text{PMF}}(d)$ and $G_{\text{vdW}}^{\text{PMF}}(d)$ demonstrate the strong sensitivity of nonpolar hydration to local electrostatics when capillary evaporation occurs and very “soft” surfaces are present. For the surfaces resulting from the tight initials (Fig. 8), the situation is a bit less sensitive to electrostatics as the final surface is close to the molecular surface for $d_c \gtrsim 8 \text{ \AA}$.

C. Proteins BphC and p53/MDM2: Dry/wet states and charge effect

1. Two-domain protein BphC

The protein biphenyl-2,3-diol-1,2-dioxygenase (BphC) is a key enzyme of biphenyl biodegradation pathway in *Pseudomonas sp.* The functional unit of this protein is a homo-octamer, and each subunit consists of two domains. The separation of the two domains in the native configuration in crystal structure has the 0 \AA separation (PDB code: 1dhy). It

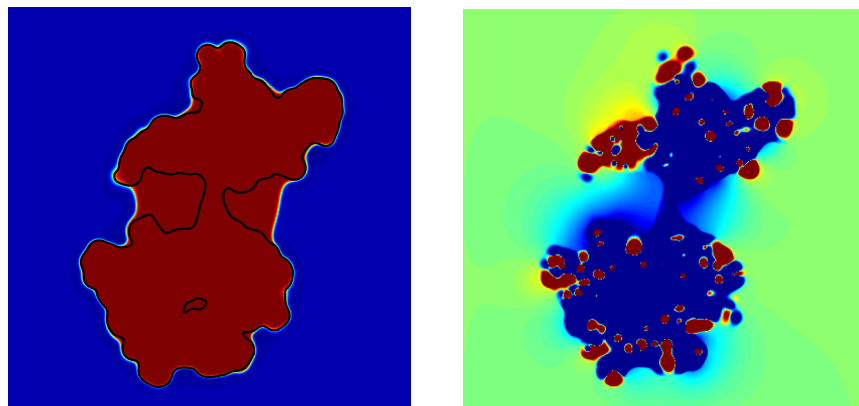


FIG. 10. Cross sections of BphC obtained by PF-VISM computation with PB electrostatics. Left: the superposition of a wet state indicated by the black curve and a dry state indicated by the color maroon using the computed phase field. Right: the electrostatic potential distribution with blue for positive and red for negative values.

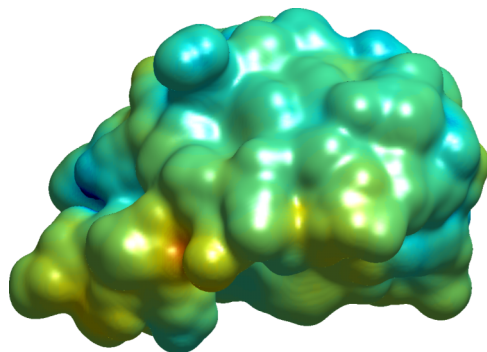


FIG. 11. A stable equilibrium conformation of the protein p53/MDM2 obtained by our PF-VISM calculation with the PB electrostatics. Color indicates the electrostatic potential distribution, with blue for positive and red for negative values.

has been shown that the behavior of water molecules between the two domains depends heavily on both nonpolar and polar interactions with the protein.³⁹ To demonstrate that our PF-VISM can describe such behavior, particularly the charge effect, here we consider the case that the two domains are separated in 14 Å. We use the following parameters in our PF-VISM calculations for this system: the effective surface tension $\gamma_0 = 0.1 k_B T / \text{Å}^2$, the bulk solvent density $\rho_w = 0.0333 \text{ Å}^{-3}$, the dielectric constants $\epsilon_p = 1$ and $\epsilon_w = 78$, the inverse Debye length $\kappa = 0.1 \text{ Å}^{-1}$, and the numerical parameter $\xi = 1 \text{ Å}$. We use the solute-solvent LJ parameters same as those in our previous works.^{67,82}

In Fig. 9, we display our PF-VISM surfaces for BphC with the two domains separated at 14 Å, without (left) and with (right) atomic partial charges. It is clear that, without the charges, the necking region between the two domains is largely dry, with water molecules being pushed away from this region. When the charges are turned on, the electrostatic force pushes the solute-solvent interface inward and the necking region is quite wet, filled with many water molecules. In Fig. 10, we show some cross sections of the same three-dimensional conformations displayed in Fig. 9. Fig. 10 (left) is the superposition of the wet state indicated by the black curve and the dry state indicated by the color maroon using the computed phase field. Fig. 10 (right) is the distribution of the corresponding electrostatic potential, with blue for positive and red for negative values, for the case with the atomic partial

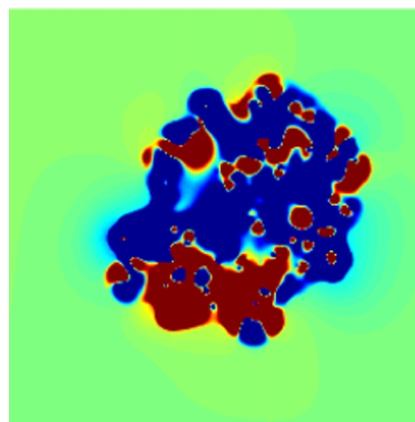


FIG. 12. A cross section of the p53/MDM2 obtained by our PF-VISM calculation with the PB electrostatics, with blue for positive and red for negative values.

charges included. We see again that the strong charge effect in pushing water molecules into the necking region.

2. The protein complex p53/MDM2

The protein p53 is known as a tumor suppressor, and the receptor protein MDM2 acts as a negative regulator of p53. Hydration of the p53/MDM2 complex plays an important role in its binding process. This system exhibits a strong hydrophobic character at the binding interface: 70% of the residues at the binding interface are apolar.^{112,113} However, the edge of the binding pocket is decorated by polar hydrophilic residues. To study the heterogeneous hydration behaviors around the protein during the p53/MDM2 binding, we choose the inter-domain distance between these two proteins to be 5 Å. We use the parameters γ_0 , ρ_w , ϵ_p , ϵ_w , κ , and ξ same as in the calculation for BphC.

In Fig. 11, we display our PF-VISM surface of the complex p53/MDM2, where the color code indicates the value of electrostatic potential, with blue for positive and red for negative values. In Fig. 12, we show the distribution of electrostatic potential in a cross section of this complex, with the same color code. In Fig. 13 (left), we show the cross section of a wet state of the system p53/MDM2 obtained by generating the vdW surface. One observes some pocket regions. In Fig. 13 (right), we show the cross section of a dry state of the system

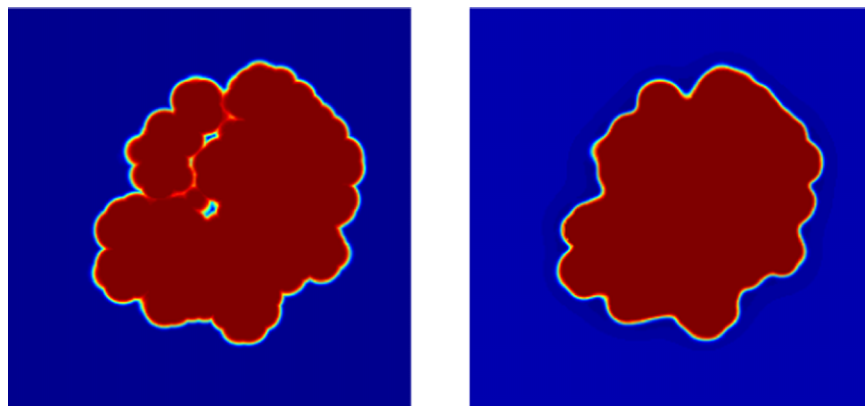


FIG. 13. A cross section of p53/MDM2 obtained by PF-VISM computation with PB electrostatics. Left: a wet state. Right: a dry state.

p53/MDM2 obtained by our PF-VISM PB calculation using a loose initial surface.

V. CONCLUSIONS

We have developed a PF-VISM with the PB electrostatics for charged molecules in aqueous solvent. Central in this model is a solvation free-energy functional of all possible phase fields, consisting of solute-solvent interfacial energy, solute excluded volume and solute-solvent vdW interaction energy, and the electrostatic free energy. We have designed, implemented, and tested efficient and accurate numerical methods for solving the gradient-flow partial differential equations to relax such a free-energy functional. Applications to the hydration of single ions, solvent-mediated interactions of two parallel plates, and solvation of protein complexes BphC and p53/MDM2 have demonstrated that our phase-field approach is a good alternative to the level-set VISM in capturing dry and wet hydration states, describing subtle electrostatic effects, and providing qualitatively good estimates of solvation free energies. Note that we do not shift our final, phase-field dielectric boundary to calculate the electrostatic free energy.

A distinguished feature of our new phase-field approach is its flexibility in describing the complex solute-solvent interfacial structure. Our PF-VISM computations of the hydration of single ions have shown that there are two different interfaces, with one closely related to the electrostatic effect. While one can question if the two boundaries will eventually merge after the code runs much longer time, it is clear that such a two-boundary interfacial structure is rather persistent. This may provide a way to resolve the boundary-shift issue in the level-set implementation, calling for further studies. Another quite different aspect of our phase-field implementation of VISM is that we need to adjust an additional numerical parameter ξ . Usually, we use $\xi = 1$ or 0.5 \AA . In principle, a very small value of ξ will lead to results that are close to those by the level-set VISM. But, for stable numerical computations in our PF-VISM with a very small ξ value, we would need to use many more spatial grid points, often not practical. Moreover, a diffuse interface will not easily move in the computation with a small ξ . A too large value of ξ may not be good either as the term $S_\xi[\phi]$ will not be close to the interfacial area. More tests are therefore needed to determine optimal values of this parameter ξ . Finally, in comparison with the level-set VISM, we have not included the curvature correction to the surface tension in our PF-VISM. Such inclusion may well increase the computational cost.^{91,114} An optimal choice of the numerical value of ξ may describe such curvature effect.

There are several issues that exist in the general VISM approach, regardless of the level-set or phase-field numerical realization. First, the efficiency of both implementations is compatible, usually ranging from minutes to hours. Due to the coupling with the electrostatics, we have to choose very small time steps in the phase-field calculations, similar to that in the level-set VISM calculations. In general, VISM is much more efficient than MD simulations, hours vs. days or weeks. But, in generating the optimal dielectric boundary, the current version of either the level-set method or our phase-field method implementing VISM is still much slower than generating a vdWS,

SES, or SAS. One possible way to speed up our computations is to use the GPU computing.

Second, VISM is an implicit-solvent model. It has a minimum number of parameters to adjust. These include the surface tension, bulk solvent density, solute and solvent dielectric coefficients, and solute-solvent LJ parameters in a forcefield of MD simulations. For nonpolar systems, such LJ parameters work well in VISM. But for charged molecules, errors can be large with using some of the LJ parameters. In addition, the charge asymmetry^{115–117} is a common issue in the continuum modeling of electrostatics. Therefore, determining VISM parameters for charged systems is important and needs to be done.

Finally, introducing the fluctuations in our VISM approach is crucial to sampling different hydration states and calculating accurately the free energy. VISM calculations can often provide quickly both tight wrap and loose wrap surfaces around an underlying charged molecule. Surface fluctuations here will then be needed only in between such VISM surfaces, making it possible to speed up the sampling process. Including such fluctuations in either the level-set or phase-field implementation of VISM amounts to solving numerically stochastic partial differential equations.¹¹⁸ We are currently working on these computational modeling and implementation.

ACKNOWLEDGMENTS

This work was supported by the National Institutes of Health (NIH) through Grant No. R01GM096188 (B.L.), the National Science Foundation (NSF) through Grant No. DMS-1319731 (B.L.), the Simons Foundation through Grant No. 357963 (Y.Z.), a start-up grant from George Washington University (Y.Z.), and the computational resources provided by the Argonne Leadership Computing Facility (ALCF), a DOE Office of Science User Facility, supported under Contract No. DE-AC02-06CH11357 (Y.Z.). Work in the McCammon group is supported in part by NSF, NIH, HHMI, and NBCR. The authors thank Dr. Jianwei Che, Dr. Li-Tien Cheng, Dr. Joachim Dzubiella, Mr. Yuan Liu, and Dr. Shenggao Zhou for many helpful discussions. They also thank Dr. Zuojun Guo for providing the data of p53/MDM2.

¹C. Tanford, *The Hydrophobic Effect: Formation of Micelles and Biological Membranes*, 2nd ed. (Wiley Interscience, 1980).

²A. Ben-Naim, *Hydrophobic Interactions* (Springer, 1980).

³B. Bagchi, "Water dynamics in the hydration layer around proteins and micelles," *Chem. Rev.* **105**(9), 3197–3219 (2003).

⁴K. A. Dill, T. M. Truskett, V. Vlachy, and B. Hribar-Lee, "Modeling water, the hydrophobic effect, and ion solvation," *Annu. Rev. Biophys. Biomol. Struct.* **34**, 173–199 (2005).

⁵Y. Levy and J. Onuchic, "Water mediation in protein folding and molecular recognition," *Annu. Rev. Biophys. Biomol. Struct.* **35**, 389–415 (2006).

⁶R. Baron and J. A. McCammon, "Molecular recognition and ligand association," *Annu. Rev. Phys. Chem.* **64**, 151–175 (2013).

⁷J. Tomasi and M. Persico, "Molecular interactions in solution: An overview of methods based on continuous distributions of the solvent," *Chem. Rev.* **94**, 2027–2094 (1994).

⁸C. J. Cramer and D. G. Truhlar, "Implicit solvation models: Equilibria, structure, spectra, and dynamics," *Chem. Rev.* **99**, 2161–2200 (1999).

⁹B. Roux and T. Simonson, "Implicit solvent models," *Biophys. Chem.* **78**, 1–20 (1999).

¹⁰M. Feig and C. L. Brooks III, "Recent advances in the development and applications of implicit solvent models in biomolecule simulations," *Curr. Opin. Struct. Biol.* **14**, 217–224 (2004).

- ¹¹N. A. Baker, "Improving implicit solvent simulations: A Poisson-centric view," *Curr. Opin. Struct. Biol.* **15**, 137–143 (2005).
- ¹²J. Chen, C. L. Brooks III, and J. Khandogin, "Recent advances in implicit solvent based methods for biomolecular simulations," *Curr. Opin. Struct. Biol.* **18**, 140–148 (2008).
- ¹³F. Fixman, "The Poisson–Boltzmann equation and its application to polyelectrolytes," *J. Chem. Phys.* **70**, 4995–5005 (1979).
- ¹⁴M. E. Davis and J. A. McCammon, "Electrostatics in biomolecular structure and dynamics," *Chem. Rev.* **90**, 509–521 (1990).
- ¹⁵K. A. Sharp and B. Honig, "Electrostatic interactions in macromolecules: Theory and applications," *Annu. Rev. Biophys. Chem.* **19**, 301–332 (1990).
- ¹⁶H. X. Zhou, "Macromolecular electrostatic energy within the nonlinear Poisson–Boltzmann equation," *J. Chem. Phys.* **100**, 3152–3162 (1994).
- ¹⁷N. A. Baker, D. Sept, S. Joseph, M. J. Holst, and J. A. McCammon, "Electrostatics of nanosystems: Application to microtubules and the ribosome," *Proc. Natl. Acad. Sci. U. S. A.* **98**, 10037–10041 (2001).
- ¹⁸F. Fogolari, A. Brigo, and H. Molinari, "The Poisson–Boltzmann equation for biomolecular electrostatics: A tool for structural biology," *J. Mol. Recognit.* **15**, 377–392 (2002).
- ¹⁹G. Lamm, "The Poisson–Boltzmann equation," in *Reviews in Computational Chemistry*, edited by K. B. Lipkowitz, R. Larter, and T. R. Cundari (Wiley, 2003), Vol. 19, pp. 147–365.
- ²⁰N. A. Baker, "Poisson–Boltzmann methods for biomolecular electrostatics," *Methods Enzymol.* **383**, 94–118 (2004).
- ²¹J. Che, J. Dzubiella, B. Li, and J. A. McCammon, "Electrostatic free energy and its variations in implicit solvent models," *J. Phys. Chem. B* **112**, 3058–3069 (2008).
- ²²P. Grochowski and J. Trylska, "Continuum molecular electrostatics, salt effects and counterion binding. A review of the Poisson–Boltzmann model and its modifications," *Biopolymers* **89**, 93–113 (2008).
- ²³B. Li, "Minimization of electrostatic free energy and the Poisson–Boltzmann equation for molecular solvation with implicit solvent," *SIAM J. Math. Anal.* **40**, 2536–2566 (2009).
- ²⁴Q. Cai, J. Wang, M. J. Hsieh, X. Ye, and R. Luo, "Poisson–Boltzmann implicit solvation models," *Annu. Rep. Comput. Chem.* **8**, 149–162 (2012).
- ²⁵W. C. Still, A. Tempczyk, R. C. Hawley, and T. Hendrickson, "Semi-analytical treatment of solvation for molecular mechanics and dynamics," *J. Am. Chem. Soc.* **112**, 6127–6129 (1990).
- ²⁶D. Bashford and D. A. Case, "Generalized Born models of macromolecular solvation effects," *Annu. Rev. Phys. Chem.* **51**, 129–152 (2000).
- ²⁷M. Born, "Volumen und Hydratationswärme der Ionen," *Z. Phys.* **1**, 45–48 (1920).
- ²⁸B. Lee and F. M. Richards, "The interpretation of protein structures: Estimation of static accessibility," *J. Mol. Biol.* **55**, 379–400 (1971).
- ²⁹F. M. Richards, "Areas, volumes, packing, and protein structure," *Annu. Rev. Biophys. Bioeng.* **6**, 151–176 (1977).
- ³⁰M. L. Connolly, "Analytical molecular surface calculation," *J. Appl. Crystallogr.* **16**, 548–558 (1983).
- ³¹T. J. Richmond, "Solvent accessible surface area and excluded volume in proteins. Analytical equations for overlapping spheres and implications for the hydrophobic effect," *J. Mol. Biol.* **178**, 63–89 (1984).
- ³²M. L. Connolly, "The molecular surface package," *J. Mol. Graphics* **11**, 139–141 (1992).
- ³³R. C. Tolman, "The effect of droplet size on surface tension," *J. Chem. Phys.* **17**, 333–337 (1949).
- ³⁴D. M. Huang, P. L. Geissler, and D. Chandler, "Scaling of hydrophobic solvation free energies," *J. Phys. Chem. B* **105**, 6704–6709 (2001).
- ³⁵R. Roth, Y. Harano, and M. Kinoshita, "Morphometric approach to the solvation free energy of complex molecules," *Phys. Rev. Lett.* **97**, 078101 (2006).
- ³⁶J. Chen and C. L. Brooks III, "Critical importance of length-scale dependence in implicit modeling of hydrophobic interactions," *J. Am. Chem. Soc.* **129**, 2444–2445 (2007).
- ³⁷L. Wang, R. A. Friesner, and B. J. Berne, "Hydrophobic interactions in model enclosures from small to large length scales: Nonadditivity in explicit and implicit solvent models," *Faraday Discuss.* **146**, 247–262 (2010).
- ³⁸R. G. Weiß, M. Heyden, and J. Dzubiella, "Curvature dependence of hydrophobic hydration dynamics," *Phys. Rev. Lett.* **114**, 187802 (2015).
- ³⁹R. Zhou, X. Huang, C. J. Margulis, and B. J. Berne, "Hydrophobic collapse in multidomain protein folding," *Science* **305**, 1605–1609 (2004).
- ⁴⁰P. Liu, X. Huang, R. Zhou, and B. J. Berne, "Observation of a dewetting transition in the collapse of the melittin tetramer," *Nature* **437**, 159–162 (2005).
- ⁴¹T. Koishi, S. Yoo, K. Yasuoka, X. C. Zeng, T. Narumi, R. Susukita, A. Kawai, H. Furusawa, A. Suenaga, N. Okimoto, N. Futatsugi, and T. Ebisuzaki, "Nanoscale hydrophobic interaction and nanobubble nucleation," *Phys. Rev. Lett.* **93**, 185701 (2004).
- ⁴²M. D. Collins, G. Hummer, M. L. Quillin, B. W. Matthews, and S. M. Gruner, "Cooperative water filling of a nonpolar protein cavity observed by high-pressure crystallography and simulation," *Proc. Natl. Acad. Sci. U. S. A.* **102**, 16668–16671 (2005).
- ⁴³X. Huang, R. Zhou, and B. J. Berne, "Drying and hydrophobic collapse of paraffin plates," *J. Phys. Chem. B* **109**, 3546–3552 (2005).
- ⁴⁴P. Setny and M. Geller, "Water properties inside nanoscopic hydrophobic pocket studied by computer simulations," *J. Chem. Phys.* **125**, 144717 (2006).
- ⁴⁵N. Choudhury and B. M. Pettitt, "The dewetting transition and the hydrophobic effect," *J. Am. Chem. Soc.* **129**, 4847–4852 (2007).
- ⁴⁶H. Yin, G. Hummer, and J. C. Rasaiah, "Metastable water clusters in the nonpolar cavities of the thermostable protein tetrabrachion," *J. Am. Chem. Soc.* **129**, 7369–7377 (2007).
- ⁴⁷J. Qvist, M. Davidovic, D. Hamelberg, and B. Halle, "A dry ligand-binding cavity in a solvated protein," *Proc. Natl. Acad. Sci. U. S. A.* **105**, 6296–6301 (2008).
- ⁴⁸R. Abel, T. Young, R. Farid, B. J. Berne, and R. A. Friesner, "Role of the active-site solvent in the thermodynamics of factor Xa ligand binding," *J. Am. Chem. Soc.* **130**(13), 2817–2831 (2008).
- ⁴⁹J. C. Rasaiah, S. Garde, and G. Hummer, "Water in nonpolar confinement: From nanotubes to proteins and beyond," *Annu. Rev. Phys. Chem.* **59**, 713–740 (2008).
- ⁵⁰J. Michel, J. Tirado-Rives, and W. L. Jorgensen, "Prediction of the water content in protein binding sites," *J. Phys. Chem. B* **113**, 13337–13346 (2009).
- ⁵¹R. Baron, P. Setny, and J. A. McCammon, "Water in cavity–ligand recognition," *J. Am. Chem. Soc.* **132**, 12091–12097 (2010).
- ⁵²L. Wang, B. J. Berne, and R. A. Friesner, "Ligand binding to protein-binding pockets with wet and dry regions," *Proc. Natl. Acad. Sci. U. S. A.* **108**, 1326–1330 (2011).
- ⁵³T. Beuming, Y. Che, R. Able, B. Kim, V. Shanmugasundaram, and W. Sherman, "Thermodynamic analysis of water molecules at the surface of proteins and applications to binding site prediction and characterization," *Proteins* **80**, 871–883 (2012).
- ⁵⁴J. Li, J. A. Morrone, and B. J. Berne, "Are hydrodynamic interactions important in the kinetics of hydrophobic collapse?," *J. Phys. Chem. B* **116**, 11537–11544 (2012).
- ⁵⁵S. Sharma and P. G. Debenedetti, "Evaporation rate of water in hydrophobic confinement," *Proc. Natl. Acad. Sci. U. S. A.* **109**(12), 4365–4370 (2012).
- ⁵⁶P. Setny, R. Baron, P. M. Kekenus-Huskey, J. A. McCammon, and J. Dzubiella, "Solvent fluctuations in hydrophobic cavity–ligand binding kinetics," *Proc. Natl. Acad. Sci. U. S. A.* **110**(4), 1197–1202 (2013).
- ⁵⁷J. Mondal, J. A. Morrone, and B. J. Berne, "How hydrophobic drying forces impact the kinetics of molecular recognition," *Proc. Natl. Acad. Sci. U. S. A.* **110**(33), 13277–13282 (2013).
- ⁵⁸R. C. Remsinga, E. Xia, S. Vembanur, S. Sharmac, P. G. Debenedetti, S. Garde, and A. J. Patel, "Pathways to dewetting in hydrophobic confinement," *Proc. Natl. Acad. Sci. U. S. A.* **112**(27), 8181–8186 (2015).
- ⁵⁹J. Dzubiella, J. M. J. Swanson, and J. A. McCammon, "Coupling hydrophobicity, dispersion, and electrostatics in continuum solvent models," *Phys. Rev. Lett.* **96**, 087802 (2006).
- ⁶⁰J. Dzubiella, J. M. J. Swanson, and J. A. McCammon, "Coupling nonpolar and polar solvation free energies in implicit solvent models," *J. Chem. Phys.* **124**, 084905 (2006).
- ⁶¹L.-T. Cheng, J. Dzubiella, J. A. McCammon, and B. Li, "Application of the level-set method to the implicit solvation of nonpolar molecules," *J. Chem. Phys.* **127**, 084503 (2007).
- ⁶²L.-T. Cheng, Y. Xie, J. Dzubiella, J. A. McCammon, J. Che, and B. Li, "Coupling the level-set method with molecular mechanics for variational implicit solvation of nonpolar molecules," *J. Chem. Theory Comput.* **5**, 257–266 (2009).
- ⁶³L.-T. Cheng, Z. Wang, P. Setny, J. Dzubiella, B. Li, and J. A. McCammon, "Interfaces and hydrophobic interactions in receptor–ligand systems: A level-set variational implicit solvent approach," *J. Chem. Phys.* **131**, 144102 (2009).
- ⁶⁴L.-T. Cheng, B. Li, and Z. Wang, "Level-set minimization of potential controlled Hadwiger valuations for molecular solvation," *J. Comput. Phys.* **229**, 8497–8510 (2010).
- ⁶⁵S. Zhou, L.-T. Cheng, J. Dzubiella, B. Li, and J. A. McCammon, "Variational implicit solvation with Poisson–Boltzmann theory," *J. Chem. Theory Comput.* **10**, 1454–1467 (2014).

- ⁶⁶P. Setny, Z. Wang, L.-T. Cheng, B. Li, J. A. McCammon, and J. Dzubiella, "Dewetting-controlled binding of ligands to hydrophobic pockets," *Phys. Rev. Lett.* **103**, 187801 (2009).
- ⁶⁷Z. Wang, J. Che, L.-T. Cheng, J. Dzubiella, B. Li, and J. A. McCammon, "Level-set variational implicit solvation with the Coulomb-field approximation," *J. Chem. Theory Comput.* **8**, 386–397 (2012).
- ⁶⁸K. E. Rogers, J. M. Ortiz-Sánchez, R. Baron, M. Fajer, C. A. F. de Oliveira, and J. A. McCammon, "On the role of dewetting transitions in host-guest binding free energy calculations," *J. Chem. Theory Comput.* **9**(1), 46–53 (2013).
- ⁶⁹Z. Guo, B. Li, J. Dzubiella, L.-T. Cheng, J. A. McCammon, and J. Che, "Evaluation of hydration free energy by the level-set variational implicit-solvent model with the coulomb-field approximation," *J. Chem. Theory Comput.* **9**, 1778–1787 (2013).
- ⁷⁰Z. Guo, B. Li, J. Dzubiella, L.-T. Cheng, J. A. McCammon, and J. Che, "Heterogeneous hydration of p53/MDM2 complex," *J. Chem. Theory Comput.* **10**, 1302–1313 (2014).
- ⁷¹Z. Guo, B. Li, L.-T. Cheng, S. Zhou, J. Andrew McCammon, and J. Che, "Identification of protein-ligand binding sites by the level-set variational implicit solvent approach," *J. Chem. Theory Comput.* **11**, 753–765 (2015).
- ⁷²S. Zhou, L.-T. Cheng, H. Sun, J. Che, J. Dzubiella, B. Li, and J. A. McCammon, "LS-VISM: A software package for analysis of biomolecular solvation," *J. Comput. Chem.* **36**(14), 1047–1059 (2015).
- ⁷³W. Kauzmann, "Some forces in the interpretation of protein denaturation," *Adv. Protein Chem.* **14**, 1–63 (1959).
- ⁷⁴D. Chandler, "Interfaces and the driving force of hydrophobic assembly," *Nature* **437**, 640–647 (2005).
- ⁷⁵H. S. Ashbaugh and L. R. Pratt, "Colloquium: Scaled particle theory and the length scales of hydrophobicity," *Rev. Mod. Phys.* **78**, 159–178 (2006).
- ⁷⁶B. J. Berne, J. D. Weeks, and R. Zhou, "Dewetting and hydrophobic interaction in physical and biological systems," *Annu. Rev. Phys. Chem.* **60**, 85–103 (2009).
- ⁷⁷S. N. Jamadagni, R. Godawat, and S. Garde, "Hydrophobicity of proteins and interfaces: Insights from density fluctuations," *Annu. Rev. Chem. Biomol. Eng.* **2**, 147–171 (2011).
- ⁷⁸J. A. Wagoner and N. A. Baker, "Assessing implicit models for nonpolar mean solvation forces: The importance of dispersion and volume changes," *Proc. Natl. Acad. Sci. U. S. A.* **103**, 8331–8336 (2006).
- ⁷⁹P. W. Bates, Z. Chen, Y. H. Sun, G. W. Wei, and S. Zhao, "Geometric and potential driving formation and evolution of biomolecular surfaces," *J. Math. Biol.* **59**, 193–231 (2009).
- ⁸⁰Z. Chen, N. A. Baker, and G. W. Wei, "Differential geometry based solvation model I: Eulerian formulation," *J. Comput. Phys.* **229**, 8231–8258 (2010).
- ⁸¹B. Li and Y. Zhao, "Variational implicit solvation with solute molecular mechanics: From diffuse-interface to sharp-interface models," *SIAM J. Appl. Math.* **73**(1), 1–23 (2013).
- ⁸²Y. Zhao, Y. Kwan, J. Che, B. Li, and J. A. McCammon, "Phase-field approach to implicit solvation of biomolecules with Coulomb-field approximation," *J. Chem. Phys.* **139**, 024111 (2013).
- ⁸³G. H. Gilmer, W. Gilmore, J. Huang, and W. W. Webb, "Diffuse interface in a critical fluid mixture," *Phys. Rev. Lett.* **14**, 491–494 (1965).
- ⁸⁴J. B. Collins and H. Levine, "Diffuse interface model of diffusion-limited crystal growth," *Phys. Rev. B* **31**, 6119–6122 (1985).
- ⁸⁵J. S. Langer, "Models of pattern formation in first-order phase transitions," in *Directions in Condensed Matter Physics*, edited by G. Grinstein and G. Mazenko (World Scientific, 1986).
- ⁸⁶L. Gránásy, "Fundamentals of the diffuse interface theory of nucleation," *J. Phys. Chem.* **100**, 10768–10770 (1995).
- ⁸⁷D. M. Anderson, G. B. McFadden, and A. A. Wheeler, "Diffuse-interface methods in fluid mechanics," *Annu. Rev. Fluid Mech.* **30**, 139–165 (1998).
- ⁸⁸A. Karma, D. Kessler, and H. Levine, "Phase-field model of mode III dynamic fracture," *Phys. Rev. Lett.* **87**, 045501 (2001).
- ⁸⁹W. J. Boettinger, J. A. Warren, C. Beckermann, and A. Karma, "Phase-field simulation of solidification," *Annu. Rev. Mater. Res.* **32**, 163–194 (2002).
- ⁹⁰L.-Q. Chen, "Phase-field models of microstructure evolution," *Annu. Rev. Mater. Res.* **32**, 113–140 (2002).
- ⁹¹Q. Du, C. Liu, and X. Wang, "A phase field approach in the numerical study of the elastic bending energy for vesicle membranes," *J. Comput. Phys.* **198**, 450–468 (2004).
- ⁹²T. Biben, K. Kassner, and C. Misbah, "Phase-field approach to three-dimensional vesicle dynamics," *Phys. Rev. E* **72**, 041921 (2005).
- ⁹³M. Tang, W. C. Carter, and R. M. Cannon, "Diffuse interface model for structural transitions of grain boundaries," *Phys. Rev. B* **73**, 024102 (2006).
- ⁹⁴D. Shao, W.-J. Rappel, and H. Levine, "Computational model for cell morphodynamics," *Phys. Rev. Lett.* **105**, 108104 (2010).
- ⁹⁵L. Modica, "The gradient theory of phase transitions and the minimal interface criterion," *Arch. Ration. Mech. Anal.* **98**, 123–142 (1987).
- ⁹⁶P. Sternberg, "The effect of a singular perturbation on nonconvex variational problems," *Arch. Ration. Mech. Anal.* **101**, 209–260 (1988).
- ⁹⁷K. Lum, D. Chandler, and J. D. Weeks, "Hydrophobicity at small and large length scales," *J. Phys. Chem. B* **103**, 4570–4577 (1999).
- ⁹⁸J. B. Hasted, D. M. Riston, and C. H. Collie, "Dielectric properties of aqueous ionic solutions. Parts I and II," *J. Chem. Phys.* **16**, 1–21 (1948).
- ⁹⁹J. S. Rowlinson and B. Widom, *Molecular Theory of Capillarity* (Clarendon Press, 1982).
- ¹⁰⁰A. P. Willard and D. Chandler, "Instantaneous liquid interfaces," *J. Phys. Chem. B* **114**, 1954–1958 (2010).
- ¹⁰¹X. Pang and H.-X. Zhou, "Poisson–Boltzmann calculations: Van der Waals or molecular surface?," *Commun. Comput. Phys.* **13**(1), 1–12 (2013).
- ¹⁰²B. Li and Y. Liu, "Diffused solute-solvent interface with Poisson–Boltzmann electrostatics: Free-energy variation and sharp-interface limit," *SIAM J. Appl. Math.* **75**, 2072–2092 (2015).
- ¹⁰³S. Balay, S. Abhyankar, M. F. Adams, J. Brown, P. Brune, K. Buschelman, L. Dalcin, V. Eijkhout, W. D. Gropp, D. Kaushik, M. G. Knepley, L. C. McInnes, K. Rupp, B. F. Smith, S. Zampini, and H. Zhang, PETSc Web page, 2015, <http://www.mcs.anl.gov/petsc>.
- ¹⁰⁴P. Hünenberger and M. Reif, *Single-Ion Solvation: Experimental and Theoretical Approaches to Elusive Thermodynamic Quantities*, 1st ed. (Royal Society of Chemistry, 2011).
- ¹⁰⁵H. B. Cheng, L.-T. Cheng, and B. Li, "Yukawa-field approximation of electrostatic free energy and dielectric boundary force," *Nonlinearity* **24**, 3215–3236 (2011).
- ¹⁰⁶D. Horinek, S. I. Mamatkulov, and R. R. Netz, "Rational design of ion force fields based on thermodynamic solvation properties," *J. Chem. Phys.* **130**, 124507 (2009).
- ¹⁰⁷Y. Marcus, "Thermodynamics of solvation of ions. Part 5.– Gibbs free energy of hydration at 298.15 K," *J. Chem. Soc., Faraday Trans.* **87**, 2995–2999 (1991).
- ¹⁰⁸L. Wang, R. A. Friesner, and B. J. Berne, "Competition of electrostatic and hydrophobic interactions between small hydrophobes and model enclosures," *J. Phys. Chem. B* **114**, 7294–7301 (2010).
- ¹⁰⁹B. Li, X.-L. Cheng, and Z.-F. Zhang, "Dielectric boundary force in molecular solvation with the Poisson–Boltzmann free energy: A shape derivative approach," *SIAM J. Appl. Math.* **71**, 2093–2111 (2011).
- ¹¹⁰Q. Cai, X. Ye, J. Wang, and R. Luo, "Dielectric boundary forces in numerical Poisson–Boltzmann methods: Theory and numerical strategies," *Chem. Phys. Lett.* **514**, 368–373 (2011).
- ¹¹¹Q. Cai, X. Ye, and R. Luo, "Dielectric pressure in continuum electrostatic solvation of biomolecules," *Phys. Chem. Chem. Phys.* **14**, 15917–15925 (2012).
- ¹¹²M. Uesugi and G. L. Verdine, "The α -helical fxx $\phi\phi$ motif in p53: TAF interaction and discrimination by MDM2," *Proc. Natl. Acad. Sci. U. S. A.* **96**(26), 14801–14806 (1999).
- ¹¹³P. Chéne, "Inhibiting the p53-MDM2 interaction: An important target for cancer therapy," *Nat. Rev. Cancer* **3**(2), 102–109 (2003).
- ¹¹⁴T. Banham, B. Li, and Y. Zhao, "Pattern formation by phase-field relaxation of bending energy with fixed surface area and volume," *Phys. Rev. E* **90**, 033308 (2014).
- ¹¹⁵W. M. Latimer, K. S. Pitzer, and C. M. Slansky, "The free energy of hydration of gaseous ions, and the absolute potential of the normal calomel electrode," *J. Chem. Phys.* **7**, 108–111 (1939).
- ¹¹⁶A. Mukhopadhyay, A. T. Fenley, I. S. Tolokh, and A. V. Onufriev, "Charge hydration asymmetry: The basic principle and how to use it to test and improve water models," *J. Phys. Chem. B* **116**(32), 9776–9783 (2012).
- ¹¹⁷J. P. Bardhan and M. G. Knepley, "Communication: Modeling charge-sign asymmetric solvation free energies with nonlinear boundary conditions," *J. Chem. Phys.* **141**, 131103 (2014).
- ¹¹⁸A. Karma and W. J. Rappel, "Phase-field model of dendritic sidebranching with thermal noise," *Phys. Rev. E* **60**, 3614–3625 (1999).